Discussion Papers report work in progress. They are written to share ideas, concepts, and theories as well as preliminary empirical data, and have not been peer reviewed or approved for publication. Comments are welcome.

RMRS-RWU-4851 Discussion Paper

The Source of Water Supply in the United States

Thomas C. Brown
Rocky Mountain Research Station, U.S. Forest Service, Fort Collins, CO

Michael T. Hobbins and Jorge A. Ramirez
Department of Civil Engineering, Colorado State University, Fort Collins

16 September 2005

(with a minor addition and corrections on 9 December 2005)

Abstract

The quantity of water originating on each 5-km by 5-km cell across the contiguous 48 states was estimated as precipitation minus evapotranspiration (ET) using data for the period 1953-94. Precipitation was estimated using the model PRISM. ET was estimated using two models, the Advection-Aridity model and the so-called Zhang model. These models were calibrated using estimates of ET computed as precipitation minus runoff at 655 relatively undisturbed basins across the 48 states. Results of the two ET models were tested using an independent data set for the 18 water resource regions of the 48 states. The final estimates of water supply reflect a mixture of results from the two ET models.

The spatially distributed estimates of mean annual water supply were mapped over political, administrative, and land cover boundaries, allowing estimates of the amount of water originating in different parts of the country. Findings include the following: (1) across the contiguous 48 states, (a) 18% of the water supply originates on national forests and grasslands and another 6% originates on other federal lands, and (b) 53% of the water supply originates on forested land, which covers only 29% of the surface area; (2) in the 11 western contiguous states, (a) 51% of the water supply originates on national forests and grasslands and another 15% originates on all other federal lands, and (b) 65% of the water supply originates on forested land, which covers only 23% of the surface area.

Table of Contents

Introduction

Water is a critical resource. As human populations increase, careful management of our water supplies becomes ever more important, both to satisfy human needs and to protect the environments of other species. Management relies on good policy, and for good policy to emerge, policy makers need an accurate broad-scale characterization of the resource. This paper aims to provide a key element of that characterization for water—spatially explicit estimates of the U.S. water supply as it originates on the watershed.

Our fresh water supply begins as precipitation falling on our land and fresh waters. From there the water naturally has three principal destinations: the atmosphere via evapotranspiration, groundwater aquifers via infiltration, or the sea via streams and rivers. Water that evaporates or transpires has largely escaped our grasp until it falls again elsewhere as precipitation. What remains is—until it reaches the sea—available for use by humans and other species, and in a broad sense is our fresh water supply.

The approach taken here was to estimate water supply at its source as precipitation minus evapotranspiration for each point in a grid covering the contiguous 48 states (Alaska and Hawaii were excluded because of lack of comparable data). Overlaying political and land ownership boundaries or land cover delineations then allows estimation of the amount of water originating on distinct land units.

A principal focus here was land managed by the U.S. Forest Service. National forests cover only 8 percent of the land area in the contiguous 48 states. However, because they are typically located at the headwaters, national forests, especially in the West, are the source of a substantial portion of the nation's water supply. Numerous estimates of the proportion of the nation's water supply originating on national forests, and on forests in general, have been suggested over the years, but they have lacked a firm empirical basis (Gillilan and Brown, 1997). A more concerted effort was recently made by the Forest Service to determine the importance of national forests to our water supply (Sedell et al., 2000), but even that effort appears in a report that lacks careful documentation and was not subject to formal peer review. A more definitive study was needed.

Water runoff and its quality have always been an important focus of national forest management. Indeed, the first national forest preserves were specifically set aside by Congress for the protection of water and timber supplies (Forest Service Organic Act, 1905). Over the years, additional goals of national forest management, such as provision for livestock grazing and recreation, were specified by Congress. The mixture of management goals naturally causes conflicts and necessitates tradeoffs. Those tradeoffs are best considered in light of the facts as best we can understand them. Key among those facts is an accurate accounting of the portion of our water supply that originates on our national forests and other protected lands, and on forestland in general. Next we explain the methods we used to arrive at that accounting.

Methods

Our basic approach was to estimate contribution to water supply (Q) as precipitation (P) volume minus actual evapotranspiration (ET_a) volume on a mean annual basis at each 5-km x 5-km grid cell across the conterminous U.S.:[1]

$$Q = P - ET_a \tag{1}$$

Having these spatially distributed estimates of contribution to water supply at its source, boundaries were then overlaid. Aggregating estimates of Q across cells within a boundary indicates the amount of water supply originating within the designated area. Note that Q may become either surface flow or groundwater.

This approach requires models for estimating mean annual P and ET_a at the regional scale. As described below, a model for estimating P already existed, but for ET_a existing models were inadequate and an improved model was deemed necessary. Much of our effort focused on developing such a model. A subsidiary aim of the research was to develop a model for estimating ET_a at the *monthly* time scale that could be applied nationwide, which could then be used in other analyses that are not at issue here (including assessment of the effects of climate change on water supply). Thus we proceeded to develop a monthly model of ET_a. Unfortunately, as described below, the model we developed was not able to accurately estimate ET_a for some areas of the U.S. because of insufficient data. Therefore, in the end we used another model—one that estimates ET_a on a mean annual basis only and that became available after we began our work—in those locations where our monthly time-scale model had performed poorly. Both models are described below, as are methods for model calibration and testing.

Precipitation is the most commonly measured hydrologic variable, but because precipitation is highly variable, especially in mountainous regions of the country, models are needed for filling in between the locations of precipitation gages. For this purpose we selected the monthly precipitation estimates produced by the PRISM model (for Parameter-elevation Regressions on Independent Slopes Model) (Daly et al., 1994). PRISM combines climatological and topographical data to interpolate between the observations of precipitation. This model was selected because it yielded better results (i.e., lower cross-validation bias and absolute error) than kriging techniques (Daly et al., 1994), and was judged to be the best available estimate of precipitation fields, particularly over the complex terrain that dominates large portions of the western U.S. We used PRISM estimates of monthly precipitation at a 5-km level of resolution (Figure 1).

In hydrology it has been customary to model ET_a as a function of potential evapotranspiration (ET_p) and soil moisture, where ET_p is the evapotranspiration that would occur if water were not limiting.[2] In this approach, ET_p is considered an independent climatic variable, helping to determine the amount of ET_a but remaining unaffected by the amount of ET_a and thus largely constant over ranges of moisture

---

[1] Cells are actually about 4.69 km per side (22 km^2), resulting in a total of 355,044 cells across the conterminous US.

[2] Penman (1948) defined ET_p as "the amount of water transpired in unit time by a short green crop, completely shading the ground, of uniform height and never short of water."

availability at a given location. However, at regional scales, ET_p is not unaffected by ET_a. Rather, complex feedback interactions between processes governing the rates of ET_a and ET_p are established based on the degree to which the soil can satisfy the atmospheric demand for water vapor and on the resultant amount of energy available at the land-atmosphere interface. Models that incorporate these feedback mechanisms are called complementary relation models. We used one such model—the Advection-Aridity model—to estimate ET_a at the monthly time step.

In addition, we used a model recently proposed by Zhang et al. (2001), which employs a very different theoretical approach than that of the complementary relation model. It estimates mean annual ET_a using mean annual estimates of P and ET_p (or, alternatively, P and wet environment evapotranspiration, ET_w) along with a parameter to represent the dominant vegetation type. The Zhang model was used here principally because the Advection-Aridity model was suspected of poor accuracy in locations where data for model estimation and calibration were limited. We then compared the aggregate results of both models with independent estimates of available water supply at the 18 water resource regions of the conterminous U.S. This comparison allowed us to decide which of the two ET_a models was used in given locations for final estimates of water supply contribution.

The Complementary Relation Approach for Estimating ET_a

Theory

R. J. Bouchet proposed in 1963 that ET_a and ET_p were interdependent. He hypothesized that over areas of a regional size receiving a constant energy input and away from sharp environmental discontinuities, there exists a complementary feedback mechanism between ET_a and ET_p (Bouchet, 1963). If moisture is not limiting, ET_a equals ET_p at a rate referred to as ET_w. However, he posited, if moisture is limiting, all available energy not taken up by ET_a heats and dries the over-passing air, causing ET_p to rise above ET_w by the amount that ET_a falls below it. The complementary relation is then expressed as:

$$ET_a + ET_p = 2ET_w \tag{2}$$

Figure 2 illustrates the complementary relation.

To fully understand the complementary relation it is perhaps necessary to more carefully describe ET_p and ET_w. In this context, ET_p is approximated by the amount of water that would evaporate or transpire from a *small* continuously moist surface under the prevailing atmospheric and energy conditions. If this small moist surface is surrounded by a much larger moist area, ET_a equals ET_p at ET_w. However, when water in the surrounding area becomes limited, ET_a there falls below its potential, and a certain amount of energy becomes available. This energy excess increases the temperature and decreases the humidity of the over-passing air, causing evapotranspiration from the small moist surface (i.e., ET_p) to increase by an amount equal to the decrease in ET_a of the surrounding area. If water availability in the surrounding area is then increased the reverse process occurs, and ET_a of the surrounding area increases as ET_p decreases until both the surrounding area and the small surface are evaporating at the same rate, a rate equal to that of a large, wet area and known as ET_w. Thus, ET_p is not an independent causal factor, but rather reflects the prevailing conditions of moisture availability.

Complementary relation models rely largely on atmospheric observations. The models avoid the need for data on soil moisture, stomatal resistance properties of the vegetation, or other surface aridity measures because local temperature and humidity gradients in the atmospheric boundary layer respond to and reflect the presence of moisture availability at the surface. The reliance on more readily available atmospheric data makes complementary relation models good candidates for measuring ET_a at the regional scale.

Empirical Support

Absolute theoretical proof of the complementary relation hypothesis is lacking, except for proofs based on heuristic arguments (Morton, 1983) or on restrictive simplifying assumptions (e.g., Szilagyi, 2001). Indeed, some theoretical arguments (e.g., Kim and Entekhabi, 1998; McNaughton and Spriggs, 1989; Sugita et al., 2001) suggest that, in principle, the hypothesis of a 1:1 compensation of ET_a and ET_p around ET_w is only partially fulfilled. However, models based on the complementary relation hypothesis have been successfully used to make predictions of regional ET_a on different temporal scales, thereby providing indirect evidence of its validity (Brutsaert and Stricker, 1979; Hobbins, Ramirez, and Brown, 2001; Morton, 1983; Szilagyi, 2001). What was lacking was large-scale direct observational evidence of the complementary relation—evidence that does not rely on modeled estimates of ET_p or ET_w.

Hobbins et al. (2004b) provided this evidence, in the form of independent measurements of ET_a and ET_p at the annual time-step taken from areas spanning a wide range in moisture availability. To represent ET_p they used measurements of pan evaporation (ET_{pan}), and to represent ET_a they used estimates of precipitation minus runoff (ET_a*) from a surrounding basin, as described below.

ET_{pan} measurements were taken from the following two sources:

- Daily Evaporation: TD-3200, Surface Land Daily Cooperative Summary of the Day (EarthInfo, 1998a; NCDC, 2004d). For months in which more than two-thirds of the daily data were reported, the daily data were integrated to monthly data by summing and linearly scaling up for missing days, if necessary.
- Total Monthly Evaporation: TD-3220, Summary of the Month Cooperative (NCDC, 2004b).

Because of an interest in evapotranspiration trends, not at issue here, pans were used only if at least 20 annual totals were available within the period WY 1953-94. Forty-four pans with acceptable data were found (Figure 3), with an average record length of 28.4 years per pan, containing among them 1248 annual estimates.

The ET_{pan} measurements are subject to abrupt shifts due to changes in pan location or type or changes in the area near the pan. Because such changes can artificially bias trend results (Peterson et al., 1998), we performed a homogeneity analysis for each ET_{pan} time-series. The analysis adjusted for changes across the entire period of record as indicated by the metadata (NCDC, 2004a) accompanying the raw data or by statistical tests (i.e., *t*-test and double-mass curve analyses) indicating statistically significant abrupt shifts at the 95% level. In this manner 43% of the annual data were homogenized. See Hobbins et al. (2005a) for details.

The logic of using ET_a* to represent ET_a relies on expressing the natural water balance at a basin-scale as:

$$R_s + R_g = P - ET_a^* - \Delta S_s - \Delta S_g \quad (3)$$

where R represents runoff from the basin, P represents the precipitation input, ?S represents changes in storage, and the subscripts s and g indicate dynamics in the surface and groundwater domains, respectively. Assuming a stable climate and an undisturbed basin, the long-term net changes in overall basin moisture storage should be negligible (Eagleson, 1978). Thus, for a control volume including the ground surface and transpiring canopy and extending to the groundwater aquifer, the long-term, steady-state, water balance can be expressed as:

$$ET_a^* = P - R \quad (4)$$

where R now includes contributions from both surface R_s and groundwater R_g flow, and is estimated by the observed runoff.

Runoff data were extracted for USGS gages at the outlets of minimally impacted basins listed in the Hydro-Climatic Data Network (HCDN) (Hydrosphere Data Products, 1996; Slack and Landwehr, 1992). This network contains data for 1,659 gauging stations draining basins with little anthropogenic influence. Twenty-five basins located in conjunction with the annual pans of Figure 3 were selected for this test (shown in red in Figure 4). Digitized basin boundaries corresponding exactly to the areas draining to the HCDN gages, available by the National Weather Service, were used to extract data from the precipitation surfaces provided by the PRISM model described above.

Figure 5 (see also Hobbins et al., 2004b) presents the results of the test, showing 192 data pairs each consisting of an annual measure of pan evaporation (ET_{pan}) (a surrogate for ET_p) and an annual measure of ET_a* (a surrogate for ET_a) from the associated basin. Data for a single basin-pan pair line up vertically. Figure 5 closely matches the theoretical shape of the complementary relation between regional ET_p and ET_a (Figure 2). The highest values of ET_{pan} occur at the left of the graph, in water-limited environments, and are matched with the lowest values of ET_a*. Moving to the right as precipitation increases, the limitation of water gives way to a limitation of energy, and ET_{pan} decreases as ET_a* increases. ET_{pan} and ET_a* converge in the wettest basins.

The complementary relation implies that $(ET_a + ET_p) / 2ET_w = 1$. Using ET_{pan} as a surrogate for ET_p, the value of that ratio for the observations shown in Figure 5 has a mean of 1.10 and a variance of 0.02. Because the complementary relation is between ET_a and ET_p, and ET_{pan} generally exceeds ET_p (as measured from a moist land surface) by a small amount (Shuttleworth, 1992), there remains the possibility that the mean ratio is actually even closer to 1.0 than the 1.10 found using ET_{pan}. Indeed, Ramírez et al. (2005) report that if ET_p is estimated using the Penman equation (see equation 7 below), the average ratio of ET_{pan} to ET_p for the 192 data pairs is 0.83. Using that ratio of ET_{pan} to ET_p produces a $(ET_a + ET_p) / 2ET_w$ ratio of 0.985.

Such agreement of theory and observation is striking, especially for a dataset covering such a large geographical area and such a long temporal span (an entire year, a time period over which one would expect conditions to change considerably). Furthermore, the observations in Figure 5 have fundamentally different scales, in that ET_{pan} data are point observations, whereas ET_a* is an areal observation. The fact that the resulting graph so clearly represents the complementary relation despite these difficulties raises the possibility that improved data might reveal even more precisely the complementarity of actual and potential evapotranspiration. Of course, better data might also reveal exceptions to complementarity, but at this point it must be concluded that the complementary relation hypothesis has substantial empirical support.

The Advection-Aridity (AA) Model of Monthly ET_a

Several complementary relation models are now available, the most widely known of which are the Complementary Relationship Areal Evapotranspiration (CRAE) model (Morton, 1983) and the Advection-Aridity (AA) model (Brutsaert and Stricker, 1979). Hobbins, Ramirez, Brown, et al. (2001) compared these two models for ability to estimate ET_a across the U.S. and selected the AA model as the most promising approach for such an application. Hobbins, Ramirez, and Brown (2001) further developed the AA model, which is briefly described herein.

The AA approach combines the effects of regional advection on ET_p with the hypothesis of a complementary relation between ET_p and ET_a. In this model, ET_w is calculated based on derivations of the concept of equilibrium evapotranspiration under conditions of minimal advection, first proposed by Priestley and Taylor (1972), and ET_p is calculated by combining information from the energy budget and water vapor transfer in the Penman equation (Penman, 1948). ET_a is then calculated as a residual of Equation 2.

The Priestley and Taylor equation is:

$$l ET_w = a_{PT} \frac{\Delta}{\Delta + g} Q_N \quad (5)$$

where ? represents the latent heat of vaporization, ? is the slope of the saturated vapor pressure curve at air temperature, Q_N is the net energy available at the evaporating surface, and ? is the psychrometric constant. Assuming no net change in heat storage over long time periods, Q_N is as follows:

$$Q_N = \left[\left(R_D + R_H \right) \left(1 - A_{SW} \right) \right] + \left[LW \downarrow \left(1 - A_{LW} \right) - LW \uparrow \right] \quad (6)$$

where the two terms in brackets represent the short-wave and long-wave radiation balances, R_D is the direct incident solar radiation, R_H is the diffuse incident solar radiation, A_{SW} is the global short-wave albedo, A_{LW} is the long-wave albedo, LW? is the long-wave radiation from the atmosphere to the surface, and LW? is the long-wave radiation emitted by the evaporating surface.

The value of the Priestley-Taylor coefficient aPT has been studied in various land-cover types and at a range of temporal scales (e.g., DeBruin and Keijman, 1979; McNaughton and Black, 1973; Morton, 1983; Priestley and Taylor, 1972). Recognizing the variability in estimates for this empirical parameter, its calibration was the focus of much of the work in Hobbins, Ramirez, and Brown (2001), and the value obtained therein, aPT = 1.3177, was used in this study.

The familiar expression of the Penman equation for ET_p is:

$$l ET_p = \frac{\Delta}{\Delta + g} Q_N + l \frac{g}{\Delta + g} E_A \tag{7}$$

The second term of this combination approach represents the effects of large-scale advection in the transfer of water vapor, and takes the form of a scaled factor of an aerodynamic vapor transfer term E_A, also known as the “regional drying power of the air.”

The distinction between ET_a-estimation methods based on the complementary relation and those based on traditional paradigms centers on the advective component E_A. Traditional paradigms treat the over-passing air as divorced from the surface and therefore consider E_A to be independent of ET_a; a higher E_A term thus indicates that ET_a from areas upwind is lower, and vice-versa. However, with the complementary relation approach, E_A depends on ET_a. That is, E_A reflects the effects of regional advection on ET_a after the evaporating surface has been brought into equilibrium with the over-passing air by the feedbacks across the regional-scale land-surface atmosphere interface discussed in relation to equation 2. Thus, E_A is greater when there has been less evaporation into the air (due perhaps to a regional decrease in moisture availability) and the boundary layer has been well-mixed, and, conversely, decreased when regional ET_a is increased.

In either conception, however, E_A is a product of the vapor pressure deficit (e_a*–e_a) and a “wind function” of the speed of the advected air $f(U_r)$, of the form:

$$E_A = f\left(U_r\right)\left(e_a^* - e_a\right) \tag{8}$$

where U_r represents the wind speed observed at r meters above the evaporating surface, and e_a^* and e_a are the saturation vapor pressure and the actual vapor pressure of the air at r meters above the surface, respectively. The calibration of $f(U_r)$ is described in a separate section below.

Combining the expressions for E_A (Equation 8), ET_p (Equation 7), and ET_w (Equation 5) in the expression of the complementary relation (Equation 2) yields the following expression for ET_a:

$$l ET_a = \left(2a - 1\right) \frac{\Delta}{\Delta + g} Q_N - l \frac{g}{\Delta + g} f\left(U_r\right)\left(e_a^* - e_a\right) \tag{9}$$

where the two driving dynamics behind ET_a are now clear: the first term on the right represents the influence of the energy budget, and the second term represents local wetness.

Data for the AA Model

The AA model of ET_a requires data on temperature, humidity, solar radiation, wind speed, albedo, and elevation. Most of the available data are point values collected at weather stations. In order to generate spatially distributed estimates of evapotranspiration (i.e., estimates for each grid cell), spatial interpolation techniques were applied to the point observations of these variables, and evapotranspiration was then calculated at each grid cell.

Kriging was the *a priori* preference for spatial interpolation of the climatological inputs whose station networks would support the inherent semivariogram estimation procedure (Tabios and Salas, 1985). Otherwise, an inverse distance weighted (IDW) scheme was used. For each spatial variable, refinements were made to the chosen scheme in order better to describe the spatial estimates of the variables. These refinements are more fully covered in other sources (Bras and Rodriguez-Iturbe, 1993; Kitanidis, 1992; Tabios and Salas, 1985).

The point data were gathered from various sources in order to create monthly traces for the period 1953-94. The time period was limited by availability of solar radiation data. The data used for the complementary relation model are as follows:

- Average temperature was estimated as the mean of the average monthly maximum and average monthly minimum temperatures drawn from 10,176 stations in the "NCDC Summary of the Day" (EarthInfo, 1998a) database (Figure 6i). Temperature surfaces were interpolated by ordinary kriging of the station data, with the semivariogram choice optimized according to the characteristic distance method explained in Hobbins (2000).
- Humidity data, in the form of dew-point temperatures, were drawn from 324 stations in the SAMSON (NCDC, 1993) and "NCDC Surface Airways" (EarthInfo, 1998b; NCDC, 2004c) (Figure 6ii). Humidity surfaces were interpolated using ordinary kriging. These data sets contain long-term records of dew-point temperature for first and second order National Weather Service stations. The data record for most stations starts in 1948 and is updated continuously.
- Solar radiation data were drawn from 258 stations in the "Solar and Meteorological Surface Observation Network (SAMSON)" (NCDC, 1993), SOLMET (NCDC, 2001), and "NCDC Airways Solar Radiation" (EarthInfo, 1998b) databases (Figure 6iii). The development of the solar radiation input for the derivation of Q_N is described in detail in Hobbins et al. (2004a; 2005b); briefly, it is derived from the sum of diffuse radiation and direct radiation corrected for the effects of local slope and aspect. Ordinary kriging was used to produce the solar radiation surfaces.
- Wind speed data were drawn from 568 stations in the SAMSON (NCDC, 1993) and "NCDC Surface Airways" (EarthInfo, 1998b; NCDC, 2004c) databases (Figure 6iv). Most wind speed surfaces were interpolated using the inverse distance-weighted (IDW) method described in Hobbins (2000), with ordinary kriging preferred for those WRRs and months where it proved possible.
- Average monthly albedo surfaces based on Advanced Very High Resolution Radiometer (AVHRR) data were taken from Gutman (1988). The AVHRR-derived albedo estimates have an original spatial resolution of about 15-km.
- Elevation data were extracted from a 30-arc-second DEM.

The validity of calculating ET_a with interpolated observations of the meteorological variables was tested by comparing the observed relationship between average annual values of P and ET_a derived using a subset of the basins in this analysis with that derived from data obtained directly (i.e., without spatial interpolation) at the meteorological stations. Significance tests on the regression parameters of the resulting relationships indicated that those obtained for the basin subset results were not significantly different from those of the station results, thus validating this approach (Claessens, 1996).

Model Testing

The initial AA model, as first proposed by Brutsaert and Stricker (1979), was tested by comparing mean annual ET_a from the model with basin-derived estimates (ET_a*) computed as in Equation 4 (Hobbins, Ramirez, Brown et al., 2001). Runoff data were extracted for USGS gages at the outlets of 139 minimally impacted basins across the conterminous U.S. (Figure 7) included in the Hydro-Climatic Data Network (HCDN) (Hydrosphere Data Products, 1996; Slack and Landwehr, 1992) and used by Hobbins, et al. (2001; 2001) for model development and testing. Precipitation was estimated using the PRISM model as described above.

Figure 8 presents the comparison of evapotranspiration from the two sources. The test revealed considerable variance in the estimates of ET_a ($R^2 = 0.76$), and that ET_a tended to under-estimate ET_a*. Estimates of ET_p needed for predicting ET_a (see Equation 2) were determined to be the principal problem, most likely due to inadequate interpolation from weather station data.

Because of this problem, two changes were made. First, it was decided to use ET_a* to calibrate the most problematic estimate portion of the ET_p computation, the wind function. Second, additional test-basins were gathered for the calibration, bringing the total number of test-basins to 655.[3]

Model Calibration

In modeling monthly regional ET_a, the wind function is problematic because of the confounding effects of atmospheric instability acting over short time-periods and the onerous data requirements. These problems rule out theoretical formulations (e.g., Brutsaert and Stricker, 1979). Further, the empirical work done in agricultural areas to calibrate or reformulate the proposed wind function for use in the Penman equation (e.g., Allen, 1986; Wright, 1982) is of little help because of its relatively small temporal and spatial scale.

Penman (1948) originally suggested the following linear approximation for $f(U_r)$ using wind speeds measured at 2 m above the surface and therefore denoted by $f(U_2)$:

$$f\left(U_2\right) = 0.26\left(1 + 0.54U_2\right) \tag{10}$$

[3] Calibrations were also performed using ET_{pan} data (Hobbins, 2004); because these calibrations were less successful than those based on ET_a*, they are not presented here.

This formulation of $f(U_2)$ was used by Brutsaert and Stricker (1979) in their original AA model where they were operating at a temporal scale of a few days. In doing so, they ignored any effect of atmospheric stability in the wind function term.[4]

Hobbins, Ramirez, and Brown (2001) showed that the original AA model as formulated by Brutsaert and Stricker (1979), using the wind function shown in Equation 10, was strongly biased with respect to the advective input when used to estimate regional ET_a—increasingly under-estimating ET_a with increasing mean annual wind speed, especially for wind speeds above 4 m/sec. Focusing on the wind function $f(U_r)$, Hobbins, Ramirez, and Brown (2001) reparameterized and recalibrated the model on a regional, seasonal basis across the conterminous U.S. The parameterization yielded estimates of ET_a with near-zero errors when compared to independent long-term estimates of ET_a* across the original 139 test-basins (Figure 7). While these results indicated the utility of complementary relation models in general, they demonstrated the sensitivity of the performance of the AA model to the choice of formulation of *f(U2)* and the necessity to calibrate said *f(U2)* to provide spatially distributed, accurate, and unbiased estimates of ET_a.

We used a method similar to Hobbins, Ramirez, and Brown (2001). This method back-calculates values for $f(U_2)$ that are then regressed on observations of U_2 to create the two parameters (*a* and *b*, for intercept and slope, respectively) necessary to fully describe the following relation:

$$f\left(U_r\right) \approx f\left(U_2\right)_i = a_{i,basin} + b_{i,\,basin} U_2 \tag{11}$$

for the test-basins where *i* is an individual month. These parameter sets were distributed across the conterminous U.S., both within test-basins where data were available and across areas where no data were available. The AA model was then reformulated to reflect the new $f(U_2)$ relationships.

In order to optimize *a* and *b* of the linear wind function $f(U_2)$ shown in Equation 11, the following estimation procedure was adopted. It begins by specifying that, in each test-basin, the ET_a model:

$$l\,ET_a = \left(2a - 1\right)\frac{\Delta}{\Delta + g} Q_N - l\,\frac{g}{\Delta + g}\left(a + bU_2\right)\left(e_a^* - e_a\right) \tag{12}$$

(see Equation 9) matches the observations of ET_a* such that

$$ET_a = ET_a^* = P - R \tag{13}$$

as in Equation 4. Here we reiterate that negligible net changes in overall basin moisture storage in the long-term (i.e., the climatological mean) are predicated on the assumption of stationary conditions for climatic forcing.

In order to specify consideration of a 42-year time-series, Equations 12 and 13 may be expressed in the following matrix form:

$$\mathbf{E} = \mathbf{W} + A\mathbf{X} + B\mathbf{Y} \tag{14}$$

[4] While the numerical factor in the original expression in Brutsaert and Stricker (1979) is 0.35, the factor 0.26 (see Equation 9) is used here for dimensional homogeneity in the units shown.

where:

$$\mathbf{E} = ET_{a\,i} = P_i - R_i, \quad i = 1,...,42 \tag{15}$$

$$\mathbf{W} = (2a-1)\frac{\Delta_i}{\Delta_i + g_i}\frac{Q_{N\,i}}{l}, \quad i = 1,...,42 \tag{16}$$

$$\mathbf{X} = l\,\frac{g_i}{\Delta_i + g_i}\left(e_a^* - e_a\right)_i, \quad i = 1,...,42 \tag{17}$$

$$\mathbf{Y} = l\,\frac{g_i}{\Delta_i + g_i}\left(e_a^* - e_a\right)_i U_{2i}, \quad i = 1,...,42 \tag{18}$$

The constants A and B represent a and b in the wind function of the formulation of ET_a in Equation 12, and will preserve the long-term mean of each basin's ET_a* observations in modeled ET_a. Post-multiplying by the transposes of each of the known vectors **X** and **Y** and taking expectations yields a pair of simultaneous equations that may be used to estimate the values of the parameters A and B as functions of the variances and covariances of **W**, **X**, and **Y**.

Post-multiplying by the transposes of **X** and **Y** respectively:

$$\mathbf{EX}^T = \mathbf{WX}^T + A\mathbf{XX}^T + B\mathbf{YX}^T \tag{19}$$

and

$$\mathbf{EY}^T = \mathbf{WY}^T + A\mathbf{XY}^T + B\mathbf{YY}^T \tag{20}$$

and then taking expectations:

$$\mathrm{E}\left[\mathbf{EX}^T\right] = \mathrm{E}\left[\mathbf{WX}^T\right] + A\,\mathrm{E}\left[\mathbf{XX}^T\right] + B\,\mathrm{E}\left[\mathbf{YX}^T\right] \tag{21}$$

and

$$\mathrm{E}\left[\mathbf{EY}^T\right] = \mathrm{E}\left[\mathbf{WY}^T\right] + A\,\mathrm{E}\left[\mathbf{XY}^T\right] + B\,\mathrm{E}\left[\mathbf{YY}^T\right] \tag{22}$$

or, dropping the matrix notation:

$$\mathrm{S}_{EX} = \mathrm{S}_{WX} + A\,\mathrm{S}_{XX} + B\,\mathrm{S}_{YX} \tag{23}$$

and

$$\mathrm{S}_{EY} = \mathrm{S}_{WY} + A\mathrm{S}_{XY} + B\mathrm{S}_{YY} \tag{24}$$

where, for example, S_{WX} represents the covariance matrix of the two indexed time-series W_i and X_i, and S_{XX} represents the variance matrix of the indexed time-series X_i. All covariances and variances are known. This pair of simultaneous equations permits the estimation of the values of the scalars A and B, which are then respectively the values of the intercept a and the slope b in the parameter set $\{a,b\}^{\mathrm{BASIN}}$ describing $f(U_2)$ in the basin.

To create a distributed $\{a,b\}$ parameter set—one in which each cell across the conterminous U.S. contains its own $\{a,b\}$ set and therefore its own $f(U_2)$—a combined objective-subjective technique was used. This technique used large water basins delineated by the U.S. Water Resources Council (1978). At the coarsest (2-digit) level, the Council delineated 18 water resource regions (WRRs) in the conterminous U.S. (Figure 9). These were broken down into 204 4-digit planning subregions, which were further divided into 334 6-digit accounting units. We used the accounting units and subregions for the calibration procedure, and the WRRs (as is seen later) for model testing.

A series of four layers were overlain across the conterminous U.S. describing distributed $\{a,b\}$ parameter sets derived at a variety of spatial resolutions, from that of the 655 test-basins in the finest layer to that of 4-digit subregions in the coarsest layer, with each successive layer filling in gaps in the $\{a,b\}$ parameter set distributed across the preceding finer layer:

- The first, finest layer (Figure 10(i)) consists of pixels within the 655 test-basins (Figure 4). At each test-basin, the $\{a,b\}^{\text{test-basin}}$ parameter sets are specified by applying the sequence for parameterization described above (Equations 12 to 24) using data drawn only from the test-basins.
- The second layer (Figure 10(ii)) consists of those 6-digit accounting units (65% of 334) that contain test-basins. At each of these accounting units, the $\{a,b\}^{\text{6-digit}}$ parameter sets were derived as area-weighted averages of the $\{a,b\}^{\text{test-basin}}$ data from those test-basins lying within the accounting unit.
- The third layer (Figure 10(iii)) comprises those 4-digit subregions (80% of the 204) containing test-basins, and here, the same procedure was followed, with the data used to calibrate the $\{a,b\}^{\text{4-digit}}$ parameter set being gathered from the test-basins that lay within the subregion.
- The final layer (Figure 10(iv)) consists of the remaining 4-digit subregions (20% of the 204), for which $\{a,b\}^{\text{4-digit}}$ parameter sets were estimated using area-weighted averages of the $\{a,b\}^{\text{test-basin}}$ data gathered from proximal and/or climatologically representative test-basins.

The layers were then combined in the order described with the $\{a,b\}$ parameter set for each pixel across the conterminous U.S. being drawn from the first layer in the sequence that contained information for that pixel: $\{a,b\}^{\text{test-basin}}$ over $\{a,b\}^{\text{6-digit}}$ over $\{a,b\}^{\text{4-digit}}$.

The primary assumption of the ET_a*-based calibration technique is that ET_a can be described as the difference between stationary P and R processes—both of which invoke their own uncertainties, and one of which (P) is modeled rather than observed—and that in the long-term and over integer multiples of years, storages in the basin are stationary. Although the year-to-year storage changes that are neglected in estimating annual ET_a* (Equation 13) will be non-zero and therefore will add noise to the estimates in **E**, they should be negligible in modeling ET_a on a long-term mean annual basis (i.e., climatological mean annual, or the mean over this study's 42-year time-period) for undisturbed basins.

Model Performance

The calibrated AA model was used at a monthly time-step over the period WY 1953-94, with a land-surface value for a_{PT} of 1.3177, to estimate ET_a at a 5-km resolution across the conterminous U.S. (Figure 11). The models estimates of ET_a, labeled ET_a^{AA}, show a distinct positive latitudinal gradient in the eastern U.S., with mean annual ET_a^{AA} decreasing northwards, and a spatial distribution in the western U.S. complicated by the effects of a longitudinal gradient that parallels precipitation with ET_a^{AA} decreasing in a westward direction until the West Coast region is reached, and a strong positive elevational gradient with ET_a^{AA} increasing with the increased precipitation at higher elevations. Over the entire conterminous U.S., the mean annual ET_a^{AA} is 516 mm/year.

Performance at the Test-basin Level

Figure 12 depicts the performance of the model as measured against the calibrating data (ET_a*) for the 655 test-basins. Ideally, all points would be normally distributed around on the 1:1 line. A low variance is expected because the model was calibrated using test-basin data. As expected, the model performs well: the points are clustered about the line, with relatively little scatter (R^2=0.88), suggesting that the ET_a*-based calibration of the AA model predicts ET_a fairly well, with no obvious bias over the range of observed ET_a*.

In order to gain some measure of the performance of the calibrated AA model, a water balance closure error (ET_a* minus ET_a^{AA}) was calculated for each test-basin as a percentage of average annual basinwide precipitation. This percentage (*e*) is:

$$e = \frac{\sum_{i=1}^{42}\sum_{j=1}^{12}\left(ET^{*}_{a_{(i,j)}} - ET^{AA}_{a_{(i,j)}}\right)}{\sum_{i=1}^{42}\sum_{j=1}^{12} P_{(i,j)}} \bullet 100 \qquad (25)$$

where *i* and *j* here represent the water year and water month, respectively. *e* gives the average annual error as a percentage of average annual precipitation. A negative *e* indicates an over-estimation (positive *e* indicates under-estimation) of ET_a^{AA} in the test-basin.

Figure 13 displays the relation of *e* to mean annual basin-wide precipitation (*P*) measured at each of the 655 test-basins across the conterminous U.S. Clearly, *e* does not vary systematically with *P*. Figure 14 shows the distribution of closure errors. Across the 655 test-basins the mean *e* is 0.15 (median = 0.12, standard deviation = 4.9, minimum = –47, maximum = 31). Eight-five percent of the *e* are within the range from –5 to +5. Possible explanations of non-zero *e*—not quantified in this study—are: (1) violations of the assumptions inherent in Equation 4 used to develop the ET_a* estimates, perhaps through the effects of groundwater pumping, surface-water diversions, or violations of the assumption of negligible net groundwater flow out of the basin; (2) violations of the assumption of stationarity in climatological forcing; (3) errors in the hydroclimatological record; and (4) errors induced by spatial interpolation of the climatic variables.

Figure 15 shows the spatial distribution of *e* across the test-basins used to generate the ET_a* data. Nearly all of the closure errors in the eastern two-thirds of the country are below 5%. In the western third of the country larger closure errors, especially positive ones, are more common. The mean bias towards under-estimation of ET_a by the model is evident most clearly in the Great Plains and many areas of the inland West. The basins where ET_a has been over-estimated (negative e) are scattered throughout the East, South, and Midwest, but the greatest negatives are found in the Pacific Northwest.

Model Supplement

Following the calibration of ET_a^{AA}, a supplement was applied to the estimated Q. This supplement, dQ, accounts for the difference between predicted ($Q^{AA} = P - ET_a^{AA}$) and observed runoff (R) at the test-basins:

$$dQ = R - Q^{AA} = R - (P - ET_a^{AA}) \tag{26}$$

A positive dQ indicates an over-estimation of ET_a, and vice-versa. Resulting contribution to water supply (Q^{AA}) is thus:

$$Q^{AA} = P - ET_a^{AA} + dQ \tag{27}$$

The supplement dQ was computed in mm depths for each of the 655 test-basins using mean annual data, and was distributed across the conterminous U.S. using the procedure for the *{a,b}* parameter set described above, substituting dQ for *{a,b}*. Using the modeled ET_a and estimates of P derived from PRISM, it is possible to generate negative values of Q^{AA}, where ET_a^{AA} exceeds P. This situation arises where water is imported to a region where it evaporates at a higher long-term rate than the natural precipitation, as in irrigated regions, or, more widespread, through errors and inaccuracies invoked in the modeling of ET_a or P, or both. In the pixels representing such areas, and in the absence of spatially distributed, accurate, long-term data on irrigated areas, negative estimates of Q^{AA} were set to zero.

Performance at the WRR Level

Comparing modeled ET_a with ET_a* from the test-basins does not allow an independent test because the test-basins were used for model calibration. Data at the WRR level (Figure 9) allow an independent test.

The WRRs were defined for the purpose of large-scale assessment and planning. To assist such planning the U.S. Geological Survey (USGS), in the 1980s, estimated water supply available in the WRRs. Using its streamflow gage records, the USGS estimated annual outflow from the WRRs for the period 1951-83 (Graczyk et al., 1986). We averaged these annual estimates to allow a test on a mean annual basis. From the USGS estimates we subtracted inflows to WRRs 8 and 15 from upstream basins, and inflows to WRRs 9 and 17 from Canada, in order to isolate the amount of flow originating within the U.S. portions of the respective WRRs. The adjustments for WRRs 9 and 17 were based on the relative portion of the source area existing in Canada.[5] Adjustments were then made for ground water depletions (*GD*), reservoir evaporation (*RE*), and consumptive use from diversions (*CU*) based on information from Foxworthy and Moody (1986).[6] Finally, adjustments were made for interbasin transfers, specified as net imports

---

[5] A similar adjustment was not applied to WRR 13, which receives some inflow from Mexico. There remains some uncertainty about whether an adjustment is needed there.

[6] ET_a estimated using the AA model would typically capture the effects of anthropomorphic interferences such as reservoir evaporation and groundwater pumping for agricultural irrigation. However, our ET_a^{AA} estimates were calibrated based on runoff data from relatively unmolested test-basins, interfering with the

(*IM*) herein, based on data provided by Peach (1985) and Mooty and Jeffcoat (1986). Because these two sources estimated transfers for 1973-82, the mean annual transfer was necessarily assumed to apply to the entire period of interest, 1951-83. The procedure is summarized as follows:

$$Q^{USGS} = R - GD + RE + CU - IM \tag{28}$$

where R is outflow from the U.S. portion of the basin adjusted for natural inflows from elsewhere.[7] The resulting estimates of mean annual Q^{USGS} are listed in Table 3.

Estimates of mean annual Q originating in the WRRs were also computed from the monthly estimates of Q^{AA}. The WRR estimates were computed by summing across months and across the 5-km by 5-km grid cells within a WRR. The time period for these estimates, 1953-83, matched as closely as possible that of the USGS estimates (data available for the AA model did not allow including 1951 and 1952). Table 3 presents the results of this procedure.

Figure 16 presents the comparison of the two sets of estimates of mean annual Q. The overall relationship between the two sets is very good ($R^2 = 0.97$). However, on a percentage basis there are large differences for four of the drier, southwestern basins (WRRs 13-16) where the Q^{AA} appears to seriously over-estimate Q^{USGS}. This comparison is not definitive because the USGS estimates are themselves subject to substantial error. However, the relative lack of weather station and test-basin data in the Southwest for the AA model and its calibration suggest that, in these areas, improvements in estimates of model-based Q are needed.

The Zhang Model of Mean Annual ET_a

Although the AA model appeared to perform better overall than the alternatives originally considered (see the "Other Models" section below), the problem with the model in the Southwest led us to consider additional alternatives. The Zhang model (Zhang et al., 2001) was considered the best option for improving the estimates in that region. The Zhang model of mean annual ET_a is:

$$ET_a^{ZH} = P \frac{1 + wh}{1 + wh + \frac{1}{h}} \tag{29}$$

where w represents the relative amount of water used by plants and ? = ET_p/P. Following Zhang et al., we set w at 2.0 for forest cover and at 0.5 for rangeland and cropland. Following personal communication with the first author and our own testing, we replaced ET_p with ET_w, and computed ET_w as shown in Equation 5. Mean annual P was estimated using PRISM. Estimates were produced for each grid cell, both for the full study period (1953-94) and for matching the USGS data for the WRRs (1953-83).

---

ability of the model to accurately estimate such influences in areas far from the test-basins. Thus, for the WRR test we adjusted the USGS runoff estimates for major anthropomorphic influences.

[7] Adjustments were not made for the effects of filling major reservoirs, such as Lake Powell, during the 1951-83 period.

Model Testing

The Zhang model was tested by comparing mean annual ET_a from the model with basin-derived estimates (ET_a*), computed as in Equation 4, for the 655 test-basins obtained from the Hydro-Climatic Data Network (HCDN) cited above (Figure 4). As described earlier, R was taken from USGS gages and P was estimated by the PRISM model. Figure 17 compares ET_a from the two sources, revealing considerable variance in the estimates (R^2 = 0.44). Because of this variation, model estimates were adjusted, based on the ET_a* from the test-basins.

Adjustment of Model Estimates

A simple empirical approach was used for adjusting ET_a^{ZH} based on the test-basin estimates of ET_a*. The approach uses mean annual data for 1953-94 and has 3 steps.

In the first step, the 2-digit or 4-digit watersheds (WRRs or subregions, respectively) of the conterminous U.S. were separated into groups based on proximity and visual inspection of the relation of ET_a* to ET_a^{ZH} at the test-basins within the larger watersheds. Two graphs are presented here to show these relations. Figure 18 shows the test-basins east of the Rocky Mountains (in WRRs 1–12), demonstrating that the test-basins fall into three groups. Straight lines in the graphs indicate the general relationships between the two variables for the three groups. Test-basins in the Southeast (WRRs 3, 6, and 8) have relatively high ET_a levels (roughly from 600 mm to 1000 mm); here the Zhang model tends to over-estimate ET_a at the low end of the range and under-estimate ET_a at the upper end. Test-basins in the Northeast (WRRs 1 and 2) and eastern Midwest (WRRs 4 and 5) have medium ET_a levels (roughly from 400 mm to 750 mm); here the Zhang model again tends to over-estimate ET_a at the low end of the range and under-estimate ET_a at the upper end. Test-basins in the Great Plains (WRRs 10, 11 and 12) and western Midwest (WRRs 7 and 9) encompass a wide range of ET_a levels (roughly from 350 mm to 1000 mm); here the Zhang model tends to under-estimate ET_a throughout the range. Test-basins in WRRs 10 and 11 located up against the Rocky Mountains show a different relation and are not included in the figure.

Figure 19 shows the test-basins in the West (WRRs 13-18, plus basins in WRRs 10 and 11 that are up against the Rocky Mountains). Test-basins away from the West Coast (WRRs 13-16, plus the eastern portion of WRR 17) have relatively low ET_a levels (roughly from 200 mm to 600 mm); here the Zhang model tends to over-estimate ET_a but there is much scatter, especially at the lower end of the ET_a scale. Test-basins in California (WRR 18) and western Oregon and Washington (the western portion of WRR 17) contain a wide range in ET_a (roughly from 350 mm to 1200 mm); here the Zhang model poorly predicts ET_a.

In addition, a few individual 4-digit basins or small groups of 4-digit basins that did not fit with the larger groups were examined separately: these were located mostly in arid areas. For these basins we subjectively selected test-basins thought best to represent the respective 4-digit basins. Table 4 lists 2-digit or 4-digit basin groupings.

In the second step, test-basin data were used to compute coefficients for the adjustment using an OLS regression procedure wherein test-basins were the cases and all values were mean annual. For each grouping of test-basins, the ratio of ET_a* to ET_a^{ZH}

was regressed on variables selected to describe the climatology of the grouped test-basins:

$$ETratio = \frac{ET_a^*}{ET_a^{ZH}} = f\left(V_{1,}V_{2,...,}V_n\right) \quad (30)$$

where the *V*s are the spatial means across the grouped test-basins for the variables albedo (%), elevation (m), solar radiation (MJ/m^2/day), average temperature (ºC), dew point temperature (ºC), average wind speed (m/sec), and precipitation (mm). Within each test-basin group, regressing *ET ratio* on the *V*s yields a set of coefficients *b* for the *V*s. Table 4 lists the resultant coefficients along with adjusted R^2 and significance of the regressions. All regressions except that for WRR 18 and the western part of 17 are significant at <0.01.

Third, the coefficients (*b*) were applied to each grid cell within the watershed group to compute an adjusted estimate of ET_a^{ZH} labeled as ET_a^{ZHadj} :

$$ET_a^{ZHadj} = ET_a^{ZH} \bullet \left(b_0 + b_1V_1 + b_2V_2 + ... + b_vV_n\right) \quad (31)$$

Then:

$$Q^{ZH} = P - ET_a^{ZHadj} \quad (32)$$

where Q^{ZH} is adjusted Q from the Zhang model. Figure 20 displays the result of this procedure for the eastern watersheds. When compared with Figure 18, it is clear that obvious bias has been removed.

Model Performance

The adjusted Zhang model was applied using data for the period WY 1953-94 to estimate ET_a at a 5-km resolution across the conterminous U.S. (Figure 21). The model's estimates of ET_a^{ZHadj} are quite similar to those of the AA model in the East, South, and Midwest, but in the drier portions of the country the Zhang model tends to predict a considerably higher ET_a than the AA model. Over the entire conterminous U.S., the predicted mean annual ET_a^{ZHadj} is 539 mm/year.

Performance at the Test-basin Level

Figure 22 depicts the performance of the Zhang model as measured against the data used for model adjustment (ET_a*). The points are clustered along the 1:1 line with no obvious bias, but the scatter is greater (R^2 = 0.73) than with the AA model (compare to Figure 12).

Figure 23 displays the relation of e to mean annual basin-wide precipitation (P) measured at each of the 655 test-basins across the conterminous U.S. Clearly, e does not vary systematically with P. However, there is considerably more scatter than with the AA model (compare to Figure 13). Figure 24 shows the distribution of closure errors. Across the 655 test-basins the mean e is 0.22 (median = -0.08, standard deviation = 8.1, minimum = –50, maximum = 36). Only sixty-three percent of the e are within the range from –5 to +5, which again shows less precision than with the AA model (see Figure 14).

Figure 25 shows the spatial distribution of e across the test-basins used to generate the ET_a* data. In comparison with the AA model (Figure 15), the Zhang model closure errors tend to be larger, with incidences of e in excess of 5% scattered across the country. Generally in the western third of the country the closure errors tend to be less positive than with the AA model, indicating higher estimates of ET_a.

Performance at the WRR Level

As with the AA model, only the data at the WRR level allow an independent test of the Zhang model. Estimates of mean annual water supply originating in the WRRs were computed by summing Q^{ZH} across the grid cells within a WRR. The time period for these estimates, 1953-83, matched as closely as possible that of the USGS estimates. Table 3 presents the results of this procedure.

Figure 26 presents the comparison of the two sets of estimates of mean annual water supply. The overall relationship between the two sets is very good (R^2 = 0.98). Importantly, for four of the drier, southwestern basins (WRRs 13-16), Q^{ZH} are much closer to Q^{USGS} than were the AA model estimates (compare with Figure 16). The questionable quality of the Q^{USGS} estimates for these basins notwithstanding, they were significantly exceeded by the AA model, but only slightly exceeded by the Zhang model. In other words, based on the USGS estimates, the AA model tends to under-estimate ET_a in the driest basins; for example, the AA estimate of ET_a was only 64% of the Zhang estimate in WRR 15, and 70% in WRR 14 (see table 3).

Other Models

Two other ET_a models were investigated, HUMUS (Arnold et al., 1999) and MAPSS (Neilson, 1995). HUMUS estimates of mean annual Q were obtained for the 8-digit hydrologic units in the conterminous U.S. for an unspecified time period. Monthly MAPSS estimates were obtained for all 10-km by 10-km grid cells in the conterminous U.S. for the period 1961-90. From these two data sets, estimates of mean annual Q for the WRRs were computed, for comparison with Q^{USGS} of Table 3. Because the time periods of the three sets are not identical to that of the USGS estimates, the comparison is rough at best. The two R^2s for the comparison with the USGS estimates are 0.88 and 0.73, respectively, substantially lower than that reported above for the calibrated AA model or the adjusted Zhang model. Although this is not a definitive test of the four models, the results were considered sufficient to justify proceeding with the AA and Zhang models.

ET_a Model Selection

Figure 27 summarizes the findings at the WRR level of the previous sections, comparing the AA and Zhang model estimates of Q with Q^{USGS}. Table 3, right hand column, lists the percent difference in the estimates of Q from the two models. As is clearly seen in the figure and table, model results are close to the USGS estimates for most WRRs. Because the USGS estimates are undoubtedly subject to some error, small differences between the two model-based estimates for a given WRR (differences of, say, less than 10% of the USGS estimate, Table 3) do not provide substantial guidance for choosing between the models. Nevertheless, among WRRs 1-8, 17 and 18 the AA model either produces the estimate that is closer to the USGS estimate or if not then produces an estimate that is very close to the Zhang model estimate. Also, because the AA model produces generally smaller closure errors than the Zhang model, the AA model is to be preferred, all else equal. However, for WRRs 9-16 the Zhang model produces an estimate that is substantially closer to the USGS estimate than the AA model estimate. Interestingly, these eight WRRs are among the driest, all with mean annual precipitation estimates of less than 700 mm, and have substantial non-forest (largely rangeland) cover. As mentioned earlier, data for the AA model are relatively sparse on rangelands, and test-basins for calibrating the AA model are largely missing on rangelands. The models differ considerably in their estimates for rangelands but not for other cover types. Apparently the Zhang model, which attempts only to estimate mean annual ET_a, is less sensitive to data requirements and less dependent of calibration, and thus better able to estimate mean annual ET_a when data for estimation and calibration are missing.

Given this, we use the Zhang model for WRRs 9-12 and the AA model elsewhere (see Figure 31).

Administrative Boundaries and Cover Type

As a source of water supply, federal ownership was distinguished from non-federal (state and private) ownership, and then five categories of federal land management (FS, NPS, BLM, BIA, and other—assumed together to represent all federal land ownership) were tracked. The federal boundaries were taken from the Federal Lands of the United States database (U.S. Geological Survey, 2004). Because of the many small units, this coverage was modeled at a 100-m resolution. Figure 28 shows the spatial breakdown of the six ownership classes (five federal categories, plus state and private together).

The national land cover database (U.S. Geological Survey, 1992) was used to distinguish among land cover types. Five cover classes (forest, rangeland, water/wetland, agriculture, and other) were formed from the original 21 land cover classes as specified in Table 5. Figure 29 shows the spatial breakdown of the five cover classes.

Official boundaries of some states extend into major water bodies, such as the Great Lakes (e.g., Michigan) or major bays and estuaries (e.g., Washington). In these cases we clipped state boundaries at the water's edge.

Results

These results are from the combination of models described above, which is called the Mixed Model. Figure 30 shows the distribution of ET_a (from ET_a^{AA} and ET_a^{ZHadj}) and Figure 31 shows the distribution of Q (mean annual contribution to water supply) (from Q^{AA} and Q^{ZH}) across the conterminous U.S.

Nationwide

Twenty-four percent of the nation's (48 contiguous states only) water supply (429 billion m^3 per year) originates on federal land (Table 6). Eighteen percent of the nation's water supply originates on lands of the national forest system alone, although those lands occupy only about 11 percent of the surface area. Forest Service and Park Service lands yield on average 384 mm per year, while the other federal lands yield an average of only 58 mm per year and state and private lands yield an average of 238 mm per year.

Because federal lands are concentrated in the western portion of the country, the contributions of federal lands to water supply are greatest in the West. West of the Mississippi River, 42% of the nation's water supply originates on federal land, with 32% on Forest Service land alone, compared with 9% and 7%, respectively, east of the Mississippi. Or, dividing the country into four sections, we see that in the 11 western states (bordered on the east by MT, WY, CO, and NM) 66% of the water supply originates on federal lands, with 51% on Forest Service lands (although Forest Service lands occupy only about 21% of the surface area) (Table 7, Figure 32). See Table A1 a state breakdown.

Shifting to cover type, we find that 53% of the nation's water supply originates on forestland, 26% on agricultural land, and 8% on rangeland (Table 8, Figure 33). Forest is the most important cover type in most major sections of the country, contributing 65%, 56%, and 68% of the water supply in the West, South, and East, respectively (Table 9). Agricultural land is most important in the Plains and Midwest, contributing 49% and 58% of the water supply, respectively. See Table A2 for a state breakdown.

Differentiating between federal land and state and private land, we find that forest cover, nationwide, accounts for 70% of the water supply originating on federal land and 47% of the water supply originating on state and private land. See Table A3 for a state breakdown.

NFS

Total area of National Forest System (NFS) land, both national forest and grasslands, as estimated from our GIS coverage is 2% greater than the total of the official gross areas listed on the U.S. Forest Service website.[8] In this section we list water supply volume corresponding to the official gross areas and to the net NFS areas (which total 83% of gross area) from the Forest Service website. Note that tables in the previous section used the areas from the GIS federal lands coverage.

Table 10 lists the volume of water supply originating on NFS land in each of the Forest Service regions of the contiguous 48 states (Figure 34 shows the boundaries of the regions), which total to 325 billion m^3 per year using the gross area estimate. NFS parcels in Region 6 (Pacific Northwest) yield the most water of the eight NFS regions (94 billion m^3 per year using the gross area estimate), which results largely from the greater depth per acre (850 mm per year) (see Figure 35). At the other extreme, NFS parcels in Region 3 (Southwest) yield the least water (5 billion m^3 per year using the gross area estimate). Across all regions the mean depth of water supply originating on NFS land (gross area) is 387 mm per year, but the median is 330 mm per year, indicating a skewed distribution, with a few parcels located in especially wet areas (Figure 36).

[8] We generate Q-volume and parcel-area estimates using an underlying grid of Q with pixels on the order of 1000-m, which is too coarse to capture the fine-scale shapes (and hence areas) of the parcels. These errors accumulate more for parcels that are small or sinuous in shape (i.e., with large perimeter to area ratios).

About 117.8 billion m^2 of the NFS is in officially designated wilderness according to the Forest Service website (their Table 7, September 2004). Using this estimate, the total amount of water supply originating on designated NFS wilderness areas is 66.1 billion m^3 per year.

Summary

We have estimated contribution to water supply as precipitation minus evapotranspiration at each 5-km by 5-km cell across the conterminous U.S. We used two quite different evapotranspiration models (the Advection-Aridity and Zhang models) and compared our results with independent estimates for the WRRs. Based on this comparison, we selected the AA model results for 10 of the WRRs and the Zhang model results in the other 8 WRR. Overlaying land ownership and land cover type boundaries on the water supply coverage allowed estimation of the quantity of water originating in different land areas of interest.

This procedure has resulted in what are likely the most accurate estimates available so far of U.S. water supply. The estimates show that forests are the source of 53% of the U.S. water supply overall, and of fully two-thirds of the water supply in the West and South. Further, national forests and grasslands are the source of 18% of the water supply nationwide and 51% of the water supply in the West, with all other federal lands contributing another 6% and 15%, respectively.

References

Allen, R. G. 1986. A Penman for all seasons. *Journal of Irrigation and Drainage Engineering-Asce* 112(4): 348-368.

Arnold, J. G., Srinivasan, R., Mattiah, R. S., & Allen, P. M. 1999. Continental scale simulation of the hydrologic balance. *Journal of the American Water Resources Association* 35(5): 1037-1051.

Bouchet, R. J. 1963. *Evapotranspiration réelle evapotranspiration potentielle, signification climatique*. Paper presented at the International Association of Scientific Hydrology, Berkeley, CA.

Bras, R. L., & Rodriguez-Iturbe, I. 1993. *Random functions and hydrology*. Mineola, NY: Dover.

Brutsaert, W., & Stricker, H. 1979. An advection-aridity approach to estimate actual regional evapotranspiration. *Water Resources Research* 15(2): 443-450.

Claessens, L. 1996. *The complementary relationship in regional evapotranspiration and long-term large-scale water budgets*. Unpublished MS thesis, Colorado State University, Fort Collins, CO.

Daly, C., Neilson, R. P., & Phillips, D. L. 1994. A statistical-topographic model for mapping climatological precipitation over mountainous terrain. *Journal of Applied Meteorology* 33(2): 140-158.

DeBruin, H. A. R., & Keijman, J. Q. 1979. Priestley-Taylor evaporation model applied to a large, shallow lake in the Netherlands. *Journal of Applied Meteorology* 18(7): 898-903.

Eagleson, P. S. 1978. Climate, soil and vegetation, 7, A derived distribution of annual water yield. *Water Resources Research* 14(5): 765-776.

EarthInfo. 1998a. *NCDC summary of the day [TD-3200 computer file]*. Boulder, Colorado: EarthInfo, Inc.
EarthInfo. 1998b. *NCDC surface airways [TD-3200 computer file]*. Boulder, Colorado: EarthInfo, Inc.
Foxworthy, B. L., & Moody, D. W. 1986. National perspective on surface-water resources. In D. W. Moody & E. B. Chase & D. A. Aronson (Eds.), *National Water Summary 1985--Hydrologic Events and Surface-Water Resources*, Vol. Water Supply Paper 2300, pp. 51-68. Washington, D.C.: U.S. Geological Survey.
Gillilan, D. M., & Brown, T. C. 1997. *Instream flow protection: Seeking a balance in Western water use*. Washington, DC: Island Press.
Graczyk, D. J., Krug, W. R., & Gebert, W. A. 1986. *A history of annual streamflows from the 21 water-resource regions in the United States and Puerto Rico, 1951-83*. Open-File Report 86-128. Madison, WI: U.S. Geological Survey.
Gutman, G. 1988. A simple method for estimating monthly mean albedo from AVHRR data. *Journal of Applied Meteorology* 27(9): 973-988.
Hobbins, M. T. 2000. *Evaluating and enhancing two implementations of the complementary relationship in regional evapotranspiration*. Unpublished M.S. thesis, Colorado State University, Fort Collins, Colorado.
Hobbins, M. T. 2004. *Regional evapotranspiration and pan evaporation: Complementary interactions and long-term trends across the conterminous United States*. Unpublished dissertation, Colorado State University, Fort Collins, CO.
Hobbins, M. T., Ramirez, J. A., & Brown, T. C. 2001. The complementary relationship in estimation of regional evapotranspiration: An enhanced advection-aridity model. *Water Resources Research* 37(5): 1389-1403.
Hobbins, M. T., Ramirez, J. A., & Brown, T. C. 2004a. *Developing a long-term, high-resolution, continental-scale, spatially distributed time-series of topographically corrected solar radiation.* Paper presented at the Proceedings of the Twenty-fourth Annual American Geophysical Union Hydrology Days., Colorado State University, Fort Collins, Colorado.
Hobbins, M. T., Ramirez, J. A., & Brown, T. C. 2004b. Trends in pan evaporation and actual evaporation across the conterminous U.S.: Paradoxical or complementary? *Geophysical Research Letters* 31(13): L13503.
Hobbins, M. T., Ramirez, J. A., & Brown, T. C. 2005a. Developing a homogeneous data series of pan evaporation across the conterminous United States for analysis of long-term trends. Unpublished manuscript, Colorado State University, Fort Collins, Colorado.
Hobbins, M. T., Ramirez, J. A., & Brown, T. C. 2005b. Developing a long-term, high-resolution, continental-scale, spatially distributed time-series of topographically corrected solar radiation. Unpublished manuscript, Colorado State University, Fort Collins, Colorado.
Hobbins, M. T., Ramirez, J. A., Brown, T. C., & Claessens, L. H. J. M. 2001. The complementary relationship in estimation of regional evapotranspiration: The complementary relationship areal evapotranspiration and advection-aridity models. *Water Resources Research* 37(5): 1367-1387.
Hydrosphere Data Products. 1996. *Hydrodata USGS Daily Values, Volume 8.0.* Boulder, CO: Hydrosphere Data Products, Inc.

Kim, C. P., & Entekhabi, D. 1998. Feedbacks in the land-surface and mixed-layer energy budgets. *Boundary-Layer Meteorology* 88(1): 1-21.

Kitanidis, P. K. 1992. Geostatistics. In D. R. Maidment (Ed.), *Handbook of hydrology*, pp. 20.21-20.39. New York: McGraw-Hill.

McNaughton, K. G., & Black, T. A. 1973. Study of evapotranspiration from a Douglas-Fir forest using energy-balance approach. *Water Resources Research* 9(6): 1579-1590.

McNaughton, K. G., & Spriggs, T. W. 1989. An evaluation of the Priestley-Taylor equation and the complementary relation using results from a mixed layer model of the convective boundary layer. In T. A. Black & D. L. Spittlehouse & M. D. Novak & D. T. Price (Eds.), *Estimation of areal evapotranspiration*. Wallingford, United Kingdom: IAHS Press.

Mooty, W. B., & Jeffcoat, H. H. 1986. *Inventory of interbasin transfers of water in the eastern United States*. Open-File Report 86-148. Tuscaloosa, AL: U.S. Geological Survey.

Morton, F. I. 1983. Operational estimates of areal evapotranspiration and their significance to the science and practice of hydrology. *Journal of Hydrology* 66: 1-76.

NCDC. 1993. *Solar and Meteorological Surface Observation Network 1961-1990 (CD-ROM), Version 1.0*. Asheville, NC: National Climatic Data Center.

NCDC. 2001. *SOLMET [TD9724 computer file] Solar and Surface Observations, daily 1952-1976, SOLMET Volume 1 - User's Manual TD-9724*. Boulder, CO: National Climatic Data Center.

NCDC. 2004a. *Locate weather observation station record (http://www.ncdc.noaa.gov/oa/climate/stationlocator.html)*. Asheville, NC: National Climatic Data Center.

NCDC. 2004b. *Summary of the Month (SOM) Cooperative, TD-3220*. Asheville, NC: National Climatic Data Center.

NCDC. 2004c. *Surface airways, TD3280*. Asheville, NC: National Climatic Data Center.

NCDC. 2004d. *Surface Land Daily Cooperative Summary of the Day, TD-3200*. Asheville, NC: National Climatic Data Center.

Neilson, R. P. 1995. A model for predicting continental-scale vegetation distribution and water balance. *Ecological Applications* 5(2): 362-385.

Penman, H. L. 1948. *Natural evaporation from open water, bare soil and grass*. Paper presented at the Proceedings of the Royal Society of London, London.

Peterson, T. C., Easterling, D. R., Karl, T. R., Groisman, P., Nicholls, N., Plummer, N., Torok, S., Auer, I., Boehm, R., Gullett, D., Vincent, L., Heino, R., Tuomenvirta, H., Mestre, O., Szentimrey, T., Salinger, J., Forland, E. J., Hanssen-Bauer, I., Alexandersson, H., Jones, P., & Parker, D. 1998. Homogeneity adjustments of in situ atmospheric climate data: A review. *International Journal of Climatology* 18(13): 1493-1517.

Petsch, H. E., Jr. 1985. *Inventory of interbasin transfers of water in the western conterminous United States*. Open-File Report 85-166. Lakewood, CO: U.S. Geological Survey.

Priestley, C. H. B., & Taylor, R. J. 1972. On the assessment of surface heat flux and evaporation using large-scale parameters. *Monthly Weather Review* 100: 81-92.

Ramirez, J. A., Hobbins, M. T., & Brown, T. C. 2005. Observational evidence of the complementary relationship in regional evaporation lends strong support for Bouchet's hypothesis. *Geophysical Research Letters* 32(15): L15401.

Sedell, J., Sharpe, M., Apple, D. D., Copenhagen, M., & Furniss., M. 2000. *Water and the Forest Service*. Washington, D. C.: U. S. Forest Service.

Shuttleworth, W. J. 1992. Evaporation. In D. R. Maidment (Ed.), *Handbook of hydrology*, pp. 4.1-4.53. New York: McGraw-Hill.

Slack, J. R., & Landwehr, J. M. 1992. *Hydro-climatic data network (HCDN): A US Geological Survey streamflow data set for the United States for the study of climate variations, 1874-1988*. Open-File Report 92-129: US Geologic Survey.

Sugita, M., Usui, J., Tamagawa, I., & Kaihotsu, I. 2001. Complementary relationship with a convective boundary layer model to estimate regional evaporation. *Water Resources Research* 37(2): 353-365.

Szilagyi, J. 2001. On Bouchet's complementary hypothesis. *Journal of Hydrology* 246(1-4): 155-158.

Tabios, G. Q., & Salas, J. D. 1985. A comparative analysis of techniques for spatial interpolation of precipitation. *Water Resources Bulletin* 21(3): 365-380.

U.S. Geological Survey. 1992. *National land cover data set (updated)*. Reston, VA: U.S. Department of Interior.

U.S. Geological Survey. 2004. *Federal lands of the United States: National atlas of the United States*. 200412. Reston, VA: U.S. Department of Interior.

U.S. Water Resources Council. 1978. *The nation's water resources 1975-2000*. Washington, D.C.: Government Printing Office.

Wright, J. L. 1982. New evapo-transpiration crop coefficients. *Journal of the Irrigation and Drainage Division-Asce* 108(1): 57-74.

Zhang, L., Dawes, W. R., & Walker, G. R. 2001. Response of mean annual evapotranspiration to vegetation changes at catchment scale. *Water Resources Research* 37(3): 701-708.

Symbols

CU	Consumptive use from offstream diversions
e_a^*	Saturation vapor pressure of the air at r meters above the surface
e_a	Actual vapor pressure of the air at r meters above the surface
E_A	Regional drying power of the air
ET	Evapotranspiration
ET_a	Actual ET
ET_p	Potential ET
ET_{pan}	Pan evaporation
ET_a*	Actual basin ET estimated as $P - R$
ET_a^{AA}	Actual ET estimated using the AA (Advection-Aridity) model
ET_a^{ZH}	Actual ET estimated using the Zhang model
ET_a^{ZHadj}	Actual adjusted ET estimated using the Zhang model
GD	Ground water depletion
IM	Interbasin transfers, specified as net imports
P	Precipitation
Q	Contribution to water supply
Q^{AA}	Contribution to water supply estimated as $P - ET_a{}^{AA}$
Q^{ZN}	Contribution to water supply estimated as $P - ET_a{}^{ZNadj}$
Q^{USGS}	Contribution to water supply across a WRR estimated from USGS records
Q_N	Net available energy
R	Basin runoff
RE	Reservoir evaporation
S	Storage
U_r	Wind speed observed at r meters above the evaporating surface
a_{PT}	Priestley-Taylor coefficient
?	Latent heat of vaporization
?	Slope of the saturated vapor pressure curve at air temperature
?	Psychrometric constant
w	Relative amount of water used by plants
?	ET_p/P
e	Average annual error in estimating ET_a as a percentage of average annual P
WRR	Water resource region

Tables

Table 1. Test-basin size

Basin area (km^2)	Number of basins
0 – 1000	314
1000 – 2000	130
2000 – 3000	64
3000 – 4000	44
4000 – 5000	23
5000 – 6000	10
6000 – 7000	16
7000 – 8000	15
8000 – 9000	8
9000 – 10000	10
>10000	21
Total	655

Table 2. Test-basins by WRR

WRR	Number of basins
1. New England	36
2. Mid-Atlantic	98
3. South-Atlantic-Gulf	88
4. Great Lakes	28
5. Ohio	67
6.Tennessee	17
7. Upper Mississippi	72
8. Lower Mississippi	11
9. Souris-Red-Rainy	7
10. Missouri	44
11. Arkansas-White-Red	24
12.Texas-Gulf	18
13. Rio Grande	7
14. Upper Colorado	19
15. Lower Colorado	4
16. Great Basin	11
17. Pacific Northwest	62
18. California	42
Total	655

Table 3. Mean annual water supply (*Q*) originating on WRRs, estimated from USGS gage data for the period 1951-1983; and as $P - ET_a$, with ET_a computed using the calibrated AA and Zhang models, for the period 1953-1983

WRR	*Q* (Bm^3)			% difference from USGS[1]		% difference between models[2]
	USGS	AA model	Zhang model	AA model	Zhang model	
1. New England	107	92	91	-14	-15	1
2. Mid-Atlantic	134	120	115	-11	-14	4
3. South-Atlantic-Gulf	294	273	281	-7	-4	3
4. Great Lakes	108	96	84	-11	-23	11
5. Ohio	194	182	179	-6	-7	2
6.Tennessee	60	62	61	4	2	2
7. Upper Mississippi	107	104	105	-3	-2	1
8. Lower Mississippi	104	120	130	15	25	9
9. Souris-Red-Rainy	9	11	10	29	16	13
10. Missouri	92	120	93	29	1	29
11. Arkansas-White-Red	88	99	80	12	-9	21
12.Texas-Gulf	50	42	47	-15	-4	11
13. Rio Grande	6	21	6	260	2	258
14. Upper Colorado	18	47	20	159	13	147
15. Lower Colorado	4	44	5	934	22	912
16. Great Basin	11	31	14	167	23	144
17. Pacific Northwest	338	320	297	-5	-12	7
18. California	114	103	102	-10	-11	1
Total	1838	1885	1721	3	-6	

[1] Shading indicates the model that more closely matches the USGS estimate.

[2] Absolute difference between the AA and Zhang estimates as a percent of the USGS estimate.

Table 4. Coefficients for adjusting Zhang model estimates

WRRs (2-digit basins)	Planning subregions (4-digit basins)	No. test-basins	Coefficients for Zhang model adjustment								Adj R^2	Sign.
			Intercept	Albedo	Elevation	Precipita-tion.	Solar radiation	Tempera-ture	Dew temp.	Wind speed		
1, 2, 4, 5	All	229	-1.58308	0.02616	-0.00020	-0.00031	0.12162	0.03630	-0.00476	0.13269	0.593	2.80E-41
3, 6, 8	All	116	0.76809	0.02349	-0.00004	-0.00028	0.00712	-0.01106	0.02816	0.01771	0.597	3.59E-20
7, 9, 10, 11, 12	All in WRRs 7, 9, 12; most in WRRs 10, 11	156	0.40685	0.00524	0.00002	-0.00005	-0.01431	-0.00681	0.01464	0.21008	0.559	6.02E-25
10, 11, 13, 14, 15, 16, 17	All in WRRs 13-16; 1001, 1003-1005, 1007-1009, 1019, 1102, 1701-1707, 1712	84	1.23554	-0.00094	-0.00002	-0.00039	0.01417	-0.00858	0.02582	-0.00572	0.472	6.12E-10
17, 18	All in WRR 18; 1708-1711	70	2.37113	0.00659	-0.00041	0.00004	-0.03821	0.02568	-0.05734	-0.27310	0.008	3.85E-01
9	901	16	-2.89394	0.07731	-0.00131	0.00012	0.41839	0.01793	0.00540	-0.54852	0.927	5.03E-05
10	1006, 1010	17	4.79875	0.00251	0.00000	0.00062	-0.00371	-0.04915	0.08750	-0.69215	0.884	1.15E-04
11, 12	1104, 1112, 1208	36	0.37662	0.07143	0.00008	0.00002	-0.08819	-0.00114	0.03792	0.12992	0.653	2.28E-06
13	1302	8	1.51536			-0.00112					0.769	2.64E-03
13	1303	5	0.56994							0.12222	0.996	8.23E-05
13	1304	8	0.54433							0.12868	0.777	2.37E-03
13	1305	9	0.60851							0.11730	0.848	2.61E-04
13	1307	12	1.02564				-0.01423			0.08033	0.783	4.22E-04
15	1501, 1503-1505, 1507, 1508	7	1.21956			-0.00039					0.876	1.21E-03

Table 5. Land Cover Classes

Forest	
	41 Deciduous forest
	42 Evergreen forest
	43 Mixed forest
Rangeland	
	51 Shrubland
	71 Grasslands/herbaceous
Water/wetland	
	11 Open water
	12 Perennial ice/snow
	91 Woody wetlands
	92 Emergent herbaceous wetlands
Agriculture	
	61 Orchards/vineyards/other
	81 Pasture/hay
	82 Row crops
	83 Small grains
	84 Fallow
Other: developed/urban/barren	
	21 Low intensity residential
	22 High intensity residential
	23 Commercial/industrial/transportation
	31 Bare rock/sand/clay
	32 Quarries/strip mines/gravel pits
	33 Transitional
	85 Urban/recreational grasses

`Table 6. Water supply of the conterminous U.S. by land ownership type

	Volume		Mm/yr
	$m^3/10^9$/yr	Percent	
NFS	326	18	386
BLM	26	1	37
NPS	36	2	364
BIA	16	1	62
Other federal	24	1	141
State and private	1339	76	238
Total	1768	100	229

Table 7. **Water supply of the conterminous U.S. by land ownership type and U.S. region ($m^3/10^9$/yr)**

	West	Plains	Midwest	South	East	Total
NFS	245.2	3.4	18.6	51.9	6.6	325.7
BLM	26.0	0.0	0.0	0.0	0.0	26.0
NPS	31.7	0.2	0.5	3.5	0.4	36.3
BIA	11.7	1.7	2.1	0.3	0.2	16.0
Other federal	5.2	2.2	2.2	13.3	1.6	24.4
State and private	163.6	109.4	278.3	548.6	239.3	1339.2
Total	483.4	116.9	301.7	617.6	248.1	1767.7

West: AZ, CA, CO, ID, MT, NM, NV, OR, UT, WA, WY
Plains: KS, ND, NE, OK, SD, TX
Midwest: IA, IL, IN, MI, MN, MO, OH, WI
South: AL, AR, FL, GA, KY, LA, MS, NC, SC, TN, VA, WV
East: CT, DC, DE, MA, MD, ME, NH, NJ, NY, PA, RI, VT

Table 8. Water supply of the conterminous U.S. by land cover class

	Volume		mm/yr
	$m^3/10^9/yr$	Percent	
Forest	931	53	417
Rangeland	146	8	55
Agriculture	461	26	225
Water/wetland	137	8	307
Other	93	5	284
Total	1768	100	229

Table 9. Water supply of the conterminous U.S. by land cover type and U.S. region ($m^3/10^9/yr$)

	West	Plains	Midwest	South	East	Total
Forest	313.0	19.9	83.0	346.2	169.2	931.2
Rangeland	111.6	25.8	3.8	4.4	0.3	145.9
Agriculture	23.6	57.3	173.8	163.6	42.9	461.2
Water/wetland	7.2	8.9	29.6	73.4	17.5	136.5
Other	28.0	5.1	11.5	30.1	18.2	92.9
Total	483.4	116.9	301.7	617.6	248.1	1767.7

West: AZ, CA, CO, ID, MT, NM, NV, OR, UT, WA, WY
Plains: KS, ND, NE, OK, SD, TX
Midwest: IA, IL, IN, MI, MN, MO, OH, WI
South: AL, AR, FL, GA, KY, LA, MS, NC, SC, TN, VA, WV
East: CT, DC, DE, MA, MD, ME, NH, NJ, NY, PA, RI, VT

Table 10. Water supply ($m^3/10^9$/yr) of the NFS within the conterminous U.S. by FS region

Region	$m^3/10^9$/yr		mm/yr
	Gross area	Net area	
1. Northern	51	46	451
2. Rocky Mountain	20	18	183
3. Southwest	5	4	53
4. Intermountain	34	33	271
5. Pacific Southwest	43	36	446
6. Pacific Northwest	94	85	850
8. Southern	47	25	480
9. Northeastern	32	18	371
Total	325	265	387

Figures

Figure 1. Mean annual precipitation (*P*) for WY 1953-94 from PRISM. Also shown are the state and WRR boundaries (see Figure 9).

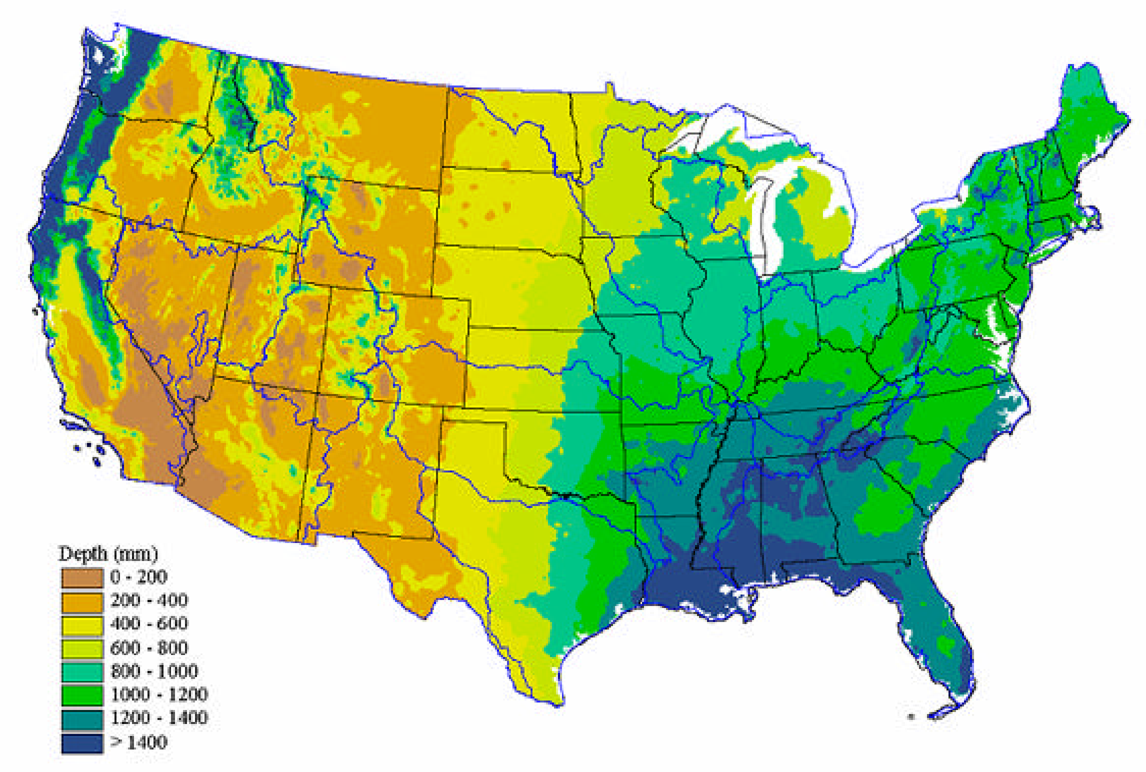

Figure 2. Schematic representation of the complementary relation in regional evapotranspiration (assuming constant energy availability)

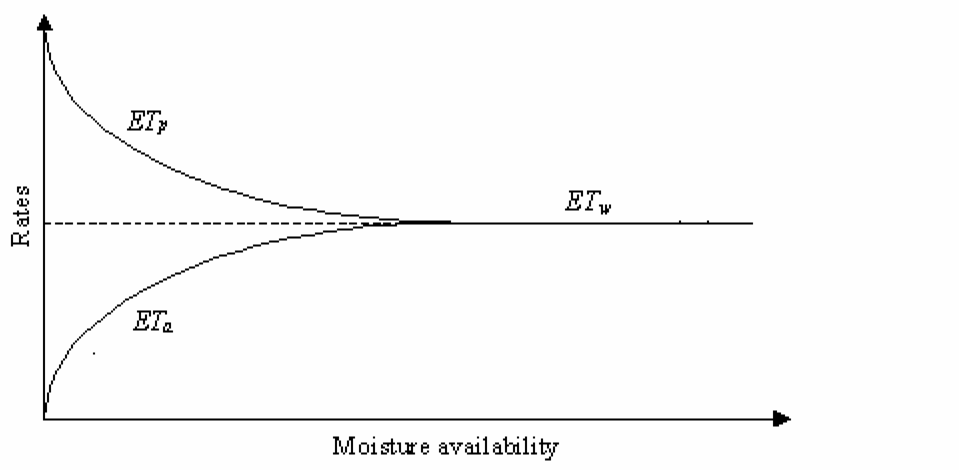

Figure 3. Location of annual pans

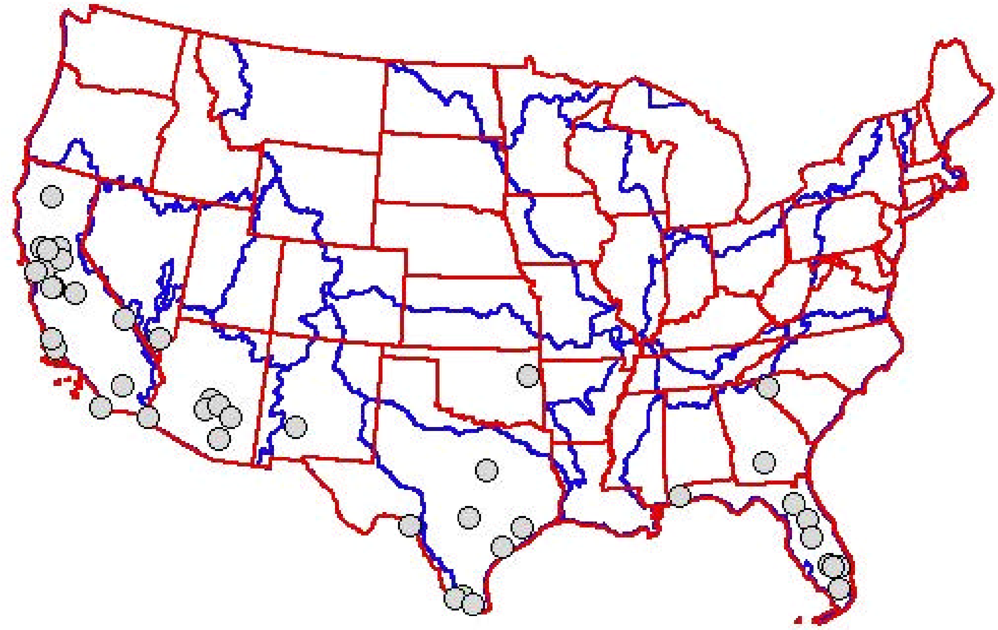

Figure 4. Locations of the 655 test-basins. ET_a* from the basins shown in red were used in Figure 5

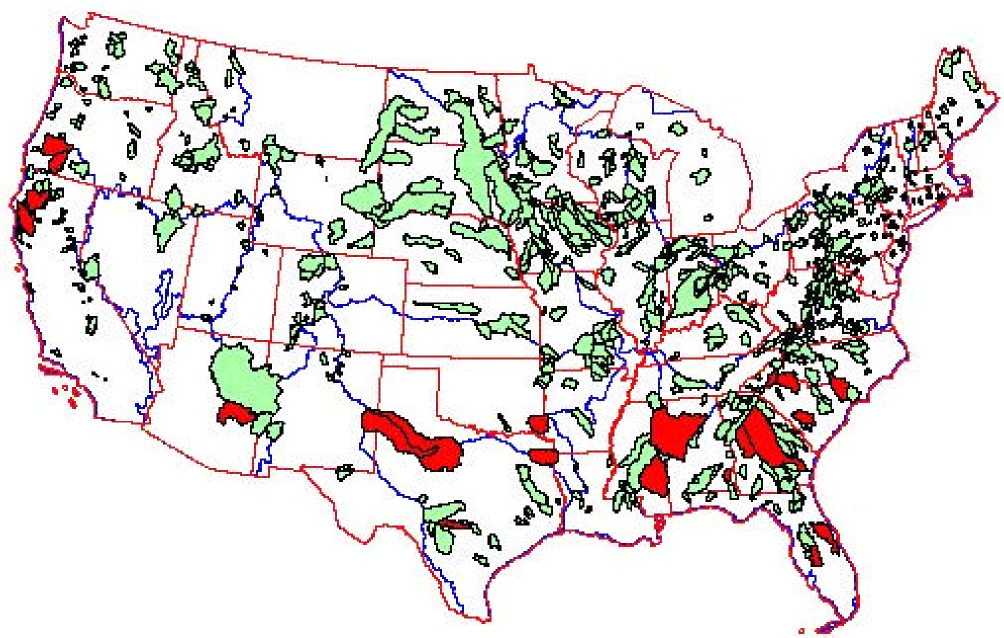

Figure 5. The observed complementary relation in point annual depths of adjusted ET_{pan} and water budget-derived, basin-wide annual depths of ET_a^* for their surrounding basins

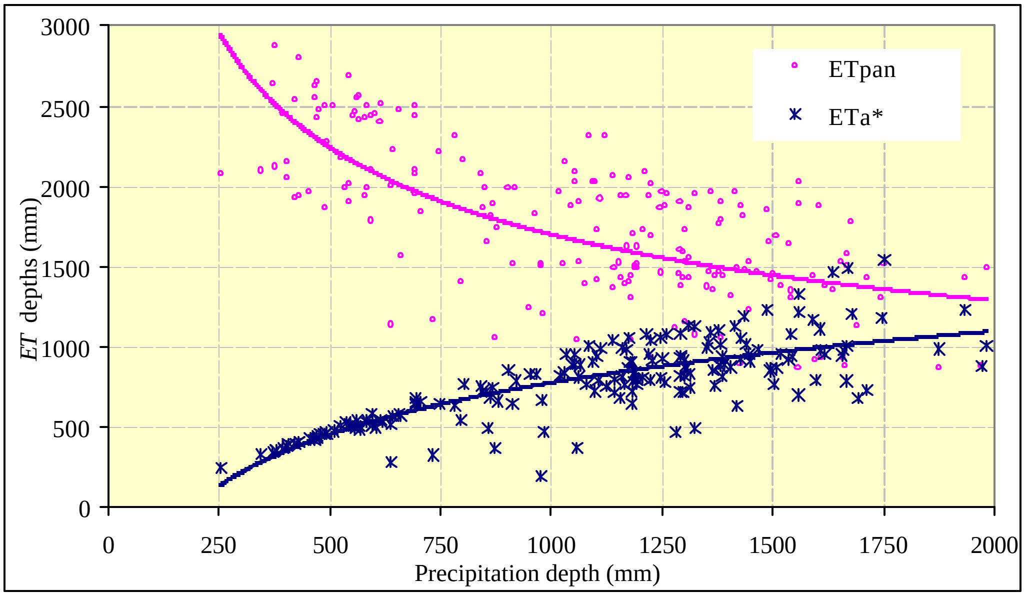

Figure 6. Locations of stations used for the following Advection-Aridity model inputs: (i) temperature; (ii) humidity; (iii) solar radiation; and (iv) wind speed

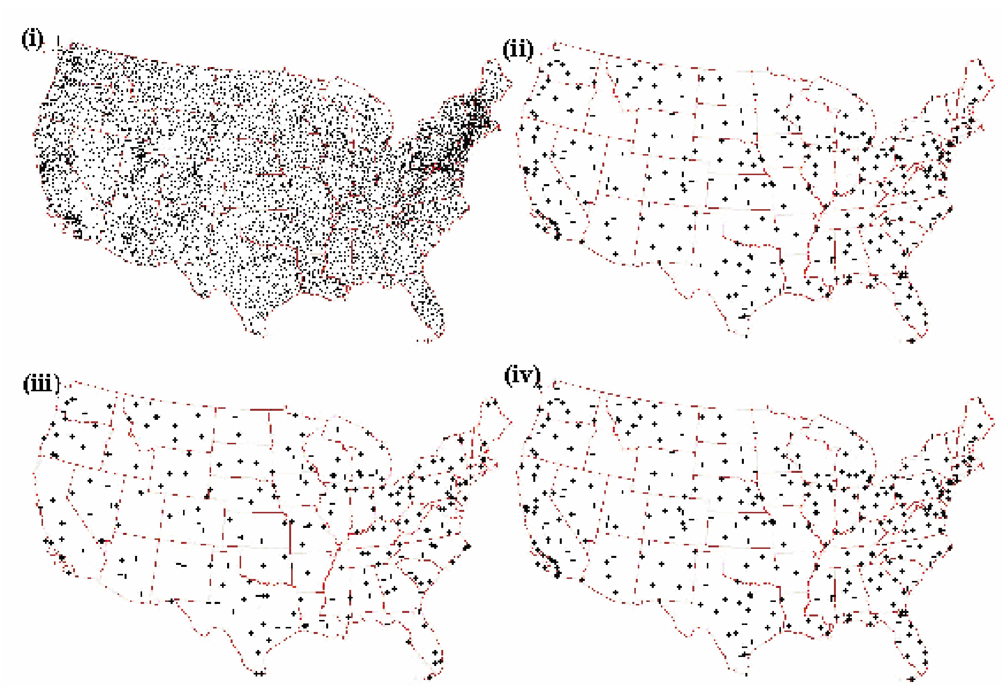

Figure 7. Original 139 basins used to test the performance of the ET_a model

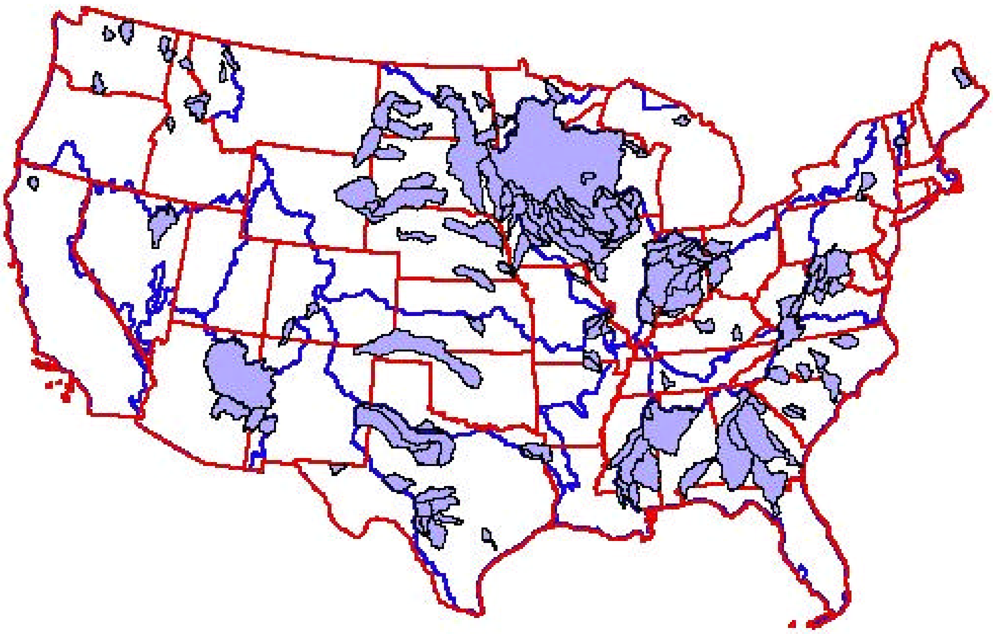

Figure 8. Mean annual ET_a depth from the AA model versus mean annual ET_a* depth for the 139 test-basins (R^2 = 0.76)

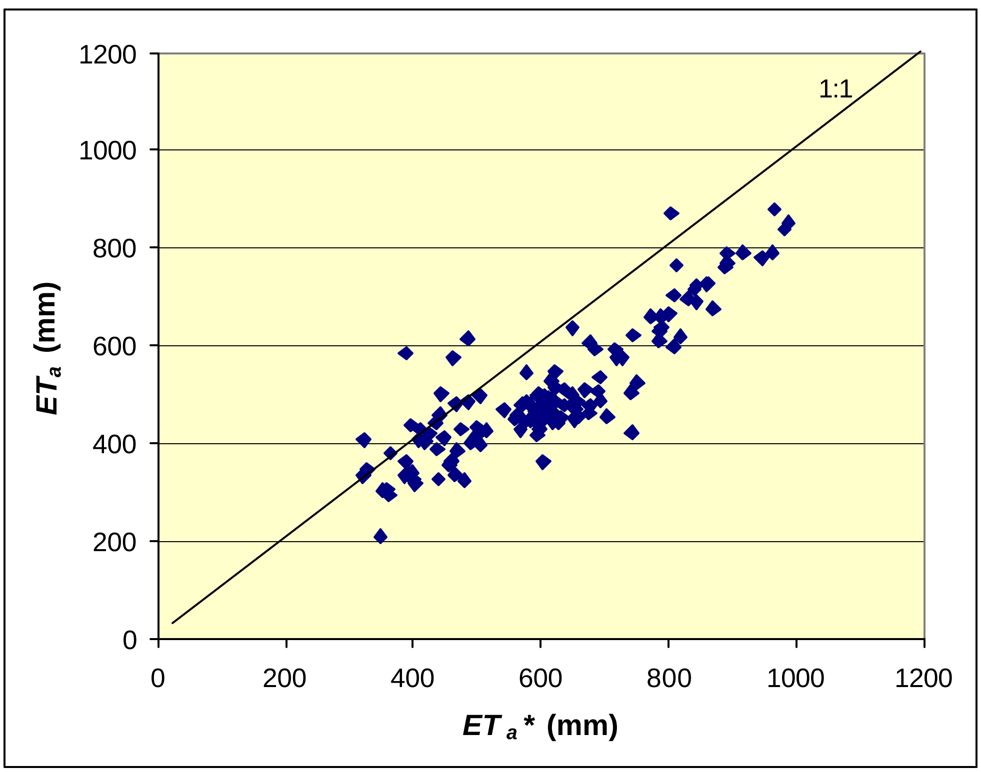

Figure 9. Water resource regions and National Forest System parcels (national forests and grasslands) in the conterminous U.S.

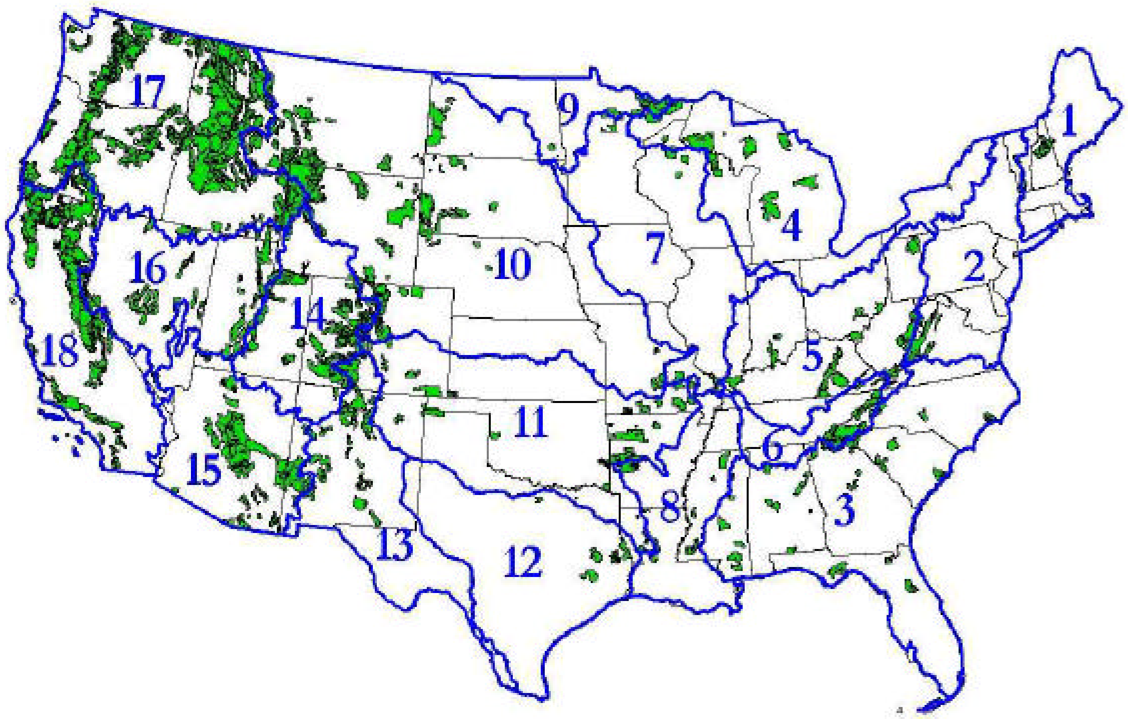

Key

1. New England
2. Mid-Atlantic
3. South-Atlantic-Gulf
4. Great Lakes
5. Ohio
6.Tennessee
7. Upper Mississippi
8. Lower Mississippi
9. Souris-Red-Rainy
10. Missouri
11. Arkansas-White-Red
12.Texas-Gulf
13. Rio Grande
14. Upper Colorado
15. Lower Colorado
16. Great Basin
17. Pacific Northwest
18. California

Figure 10. The distribution technique for ET_a*-based $f(U_2)$s. Shaded areas indicate where {*a*,*b*} parameter sets have been distributed at each stage into each of the following areas, from left to right: (i) **the test-basins;** (ii) **the 6-digit HUC-aggregates that contain test-basins;** (iii) **the 4-digit HUC-aggregates that contain test-basins; and** (iv) **all 4-digit HUC-aggregates.**

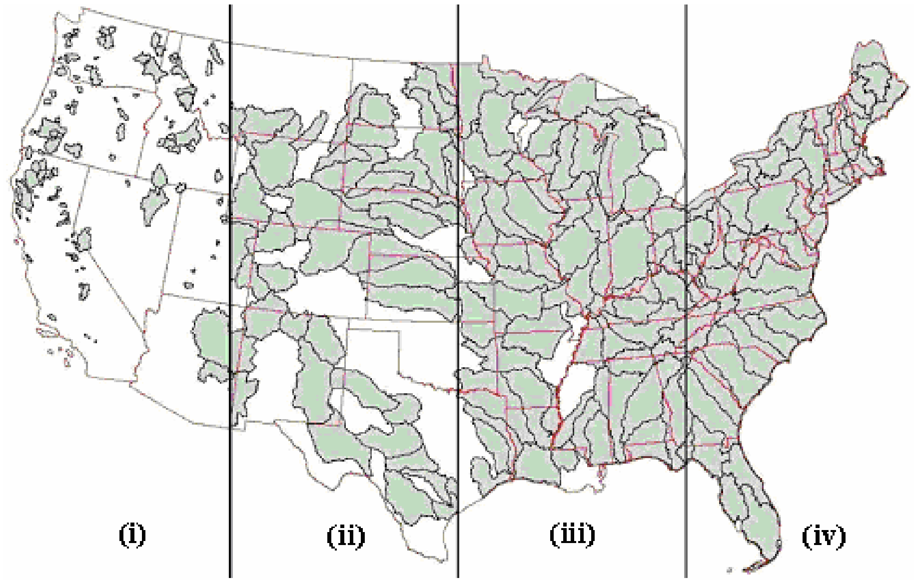

Figure 11. Distributed mean annual ET_a generated across the conterminous U.S. over 42 years using the regional, seasonal AA model with $f(U_2)$ calibrated to ET_a*.

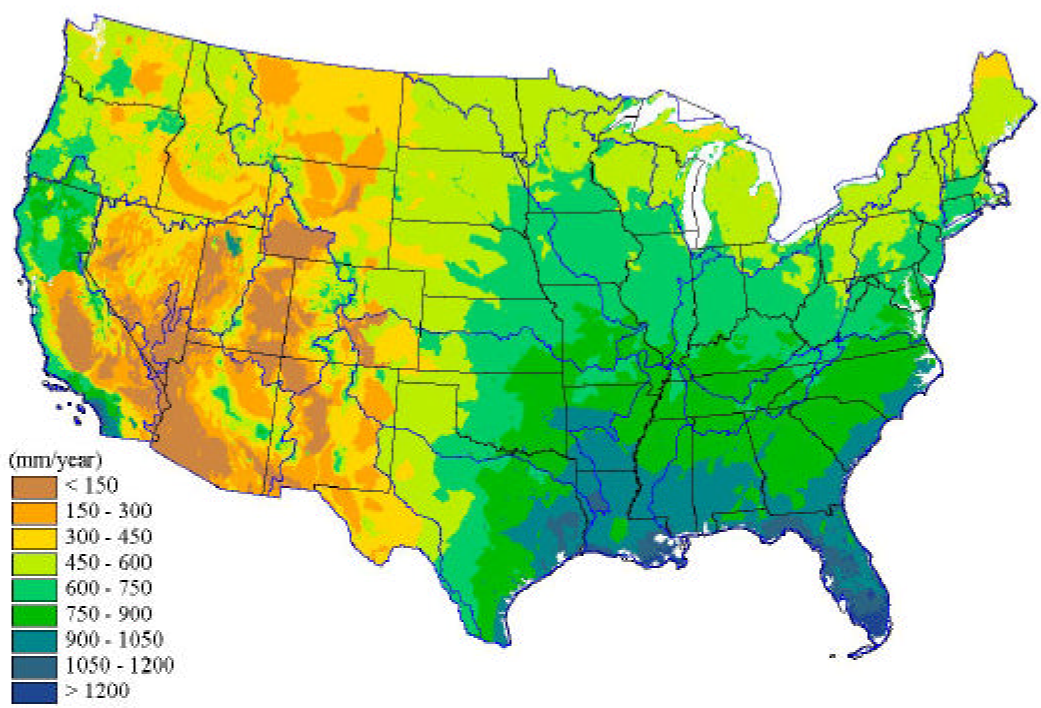

Figure 12. Mean annual ET_a depth from the calibrated AA model versus mean annual ET_a* depth for the 655 test-basins, 1953-94 (R^2 = 0.88)

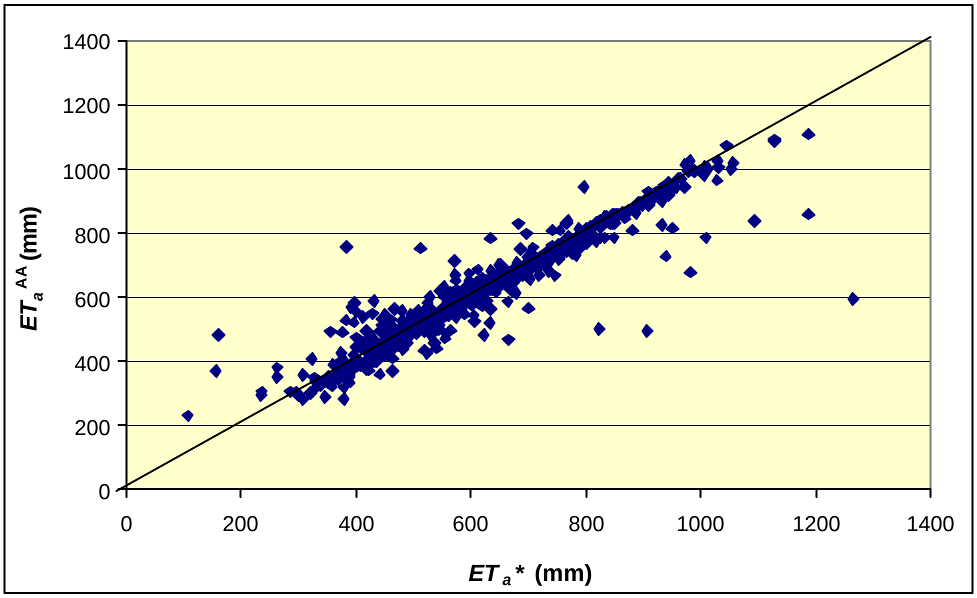

Figure 13. Mean annual ET_a closure errors for AA model versus precipitation in 655 test-basins)

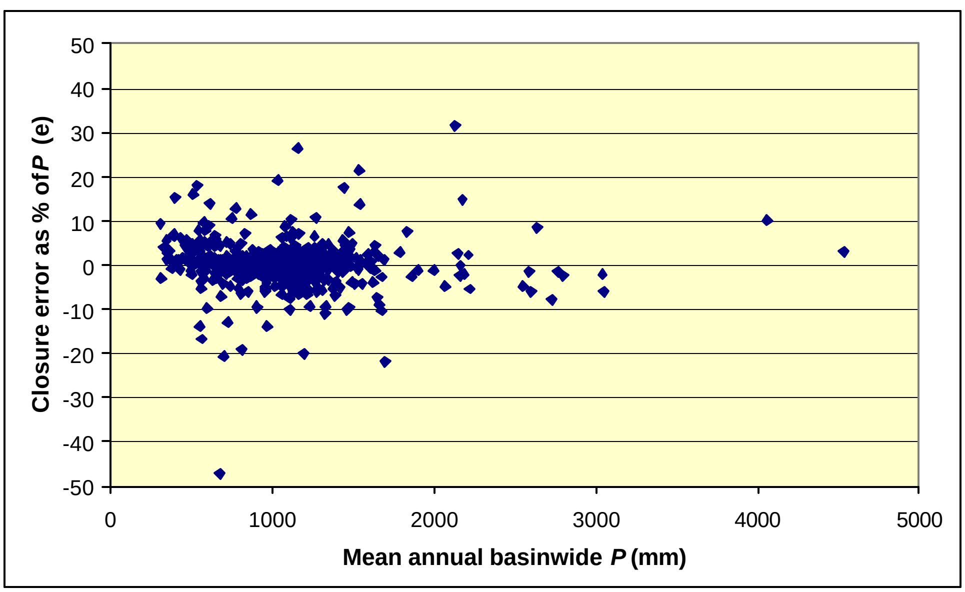

Figure 14. Distributions of mean annual closure errors for the AA model (expressed as percentages of mean annual basin-wide precipitation) at the 655 test-basins

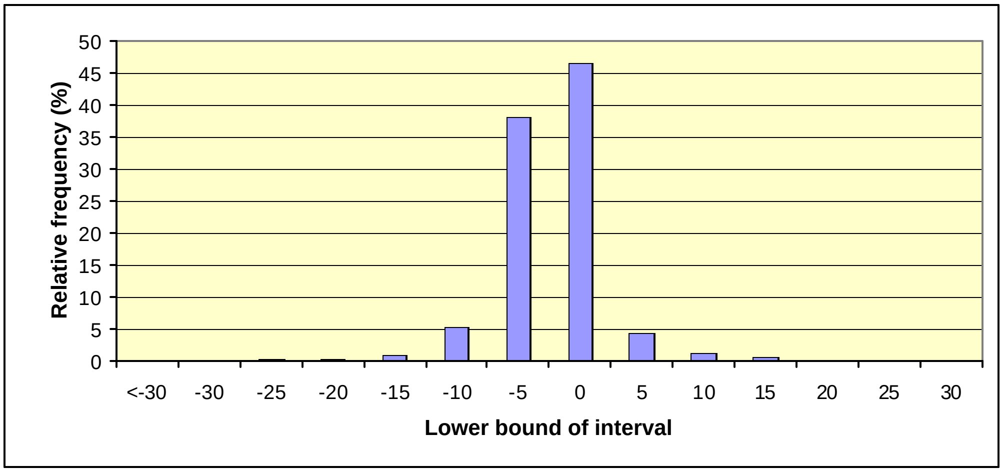

Figure 15. Spatial distribution of mean annual closure errors for the AA model (expressed as percentages of mean annual basin-wide precipitation) at the 655 test-basins.

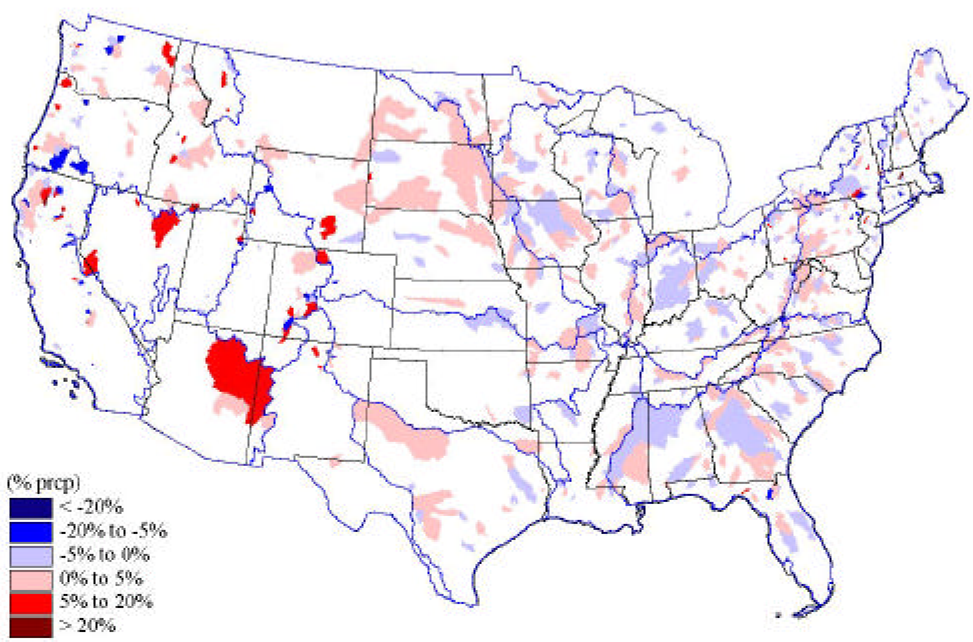

Figure 16. Mean annual *Q* for the 18 WRRs of the conterminous U.S. estimated from USGS gage data for 1951-83, and using the calibrated AA model as Q^{AA} for 1953-83 (R^2 = 0.97)

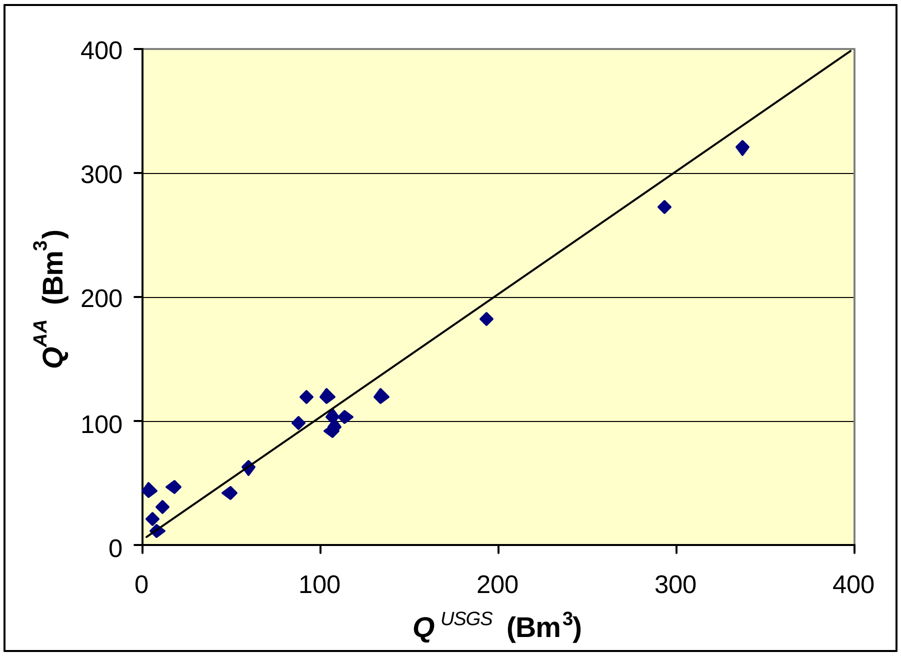

Figure 17. Mean annual ET_a depth from the Zhang model versus mean annual ET_a* depth for the 655 test-basins (R^2 = 0.44)

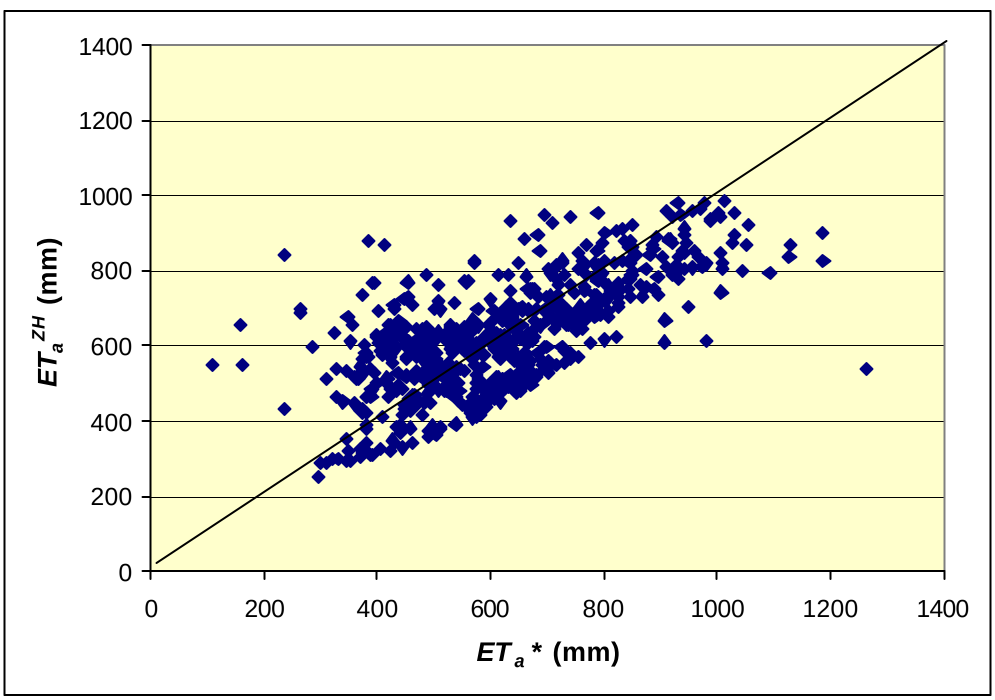

Figure 18. Mean annual ET_a depth from the Zhang model versus mean annual ET_a* depth for the 501 test-basins east of the Rockies

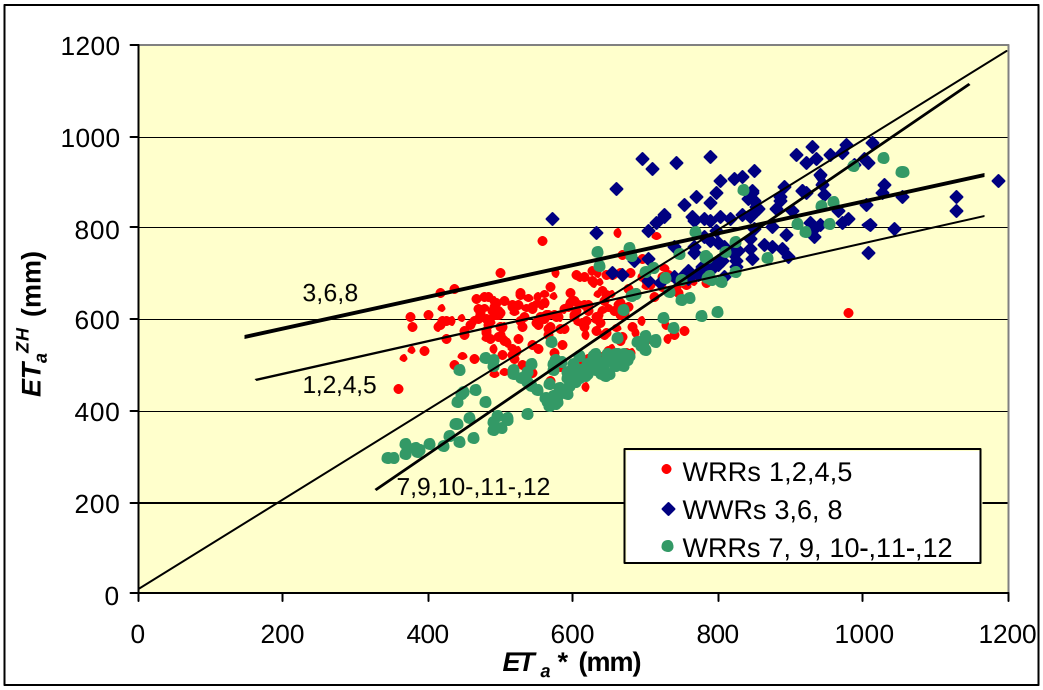

Figure 19. Mean annual ET_a depth from the Zhang model versus mean annual ET_a* depth for the 154 test-basins in the West

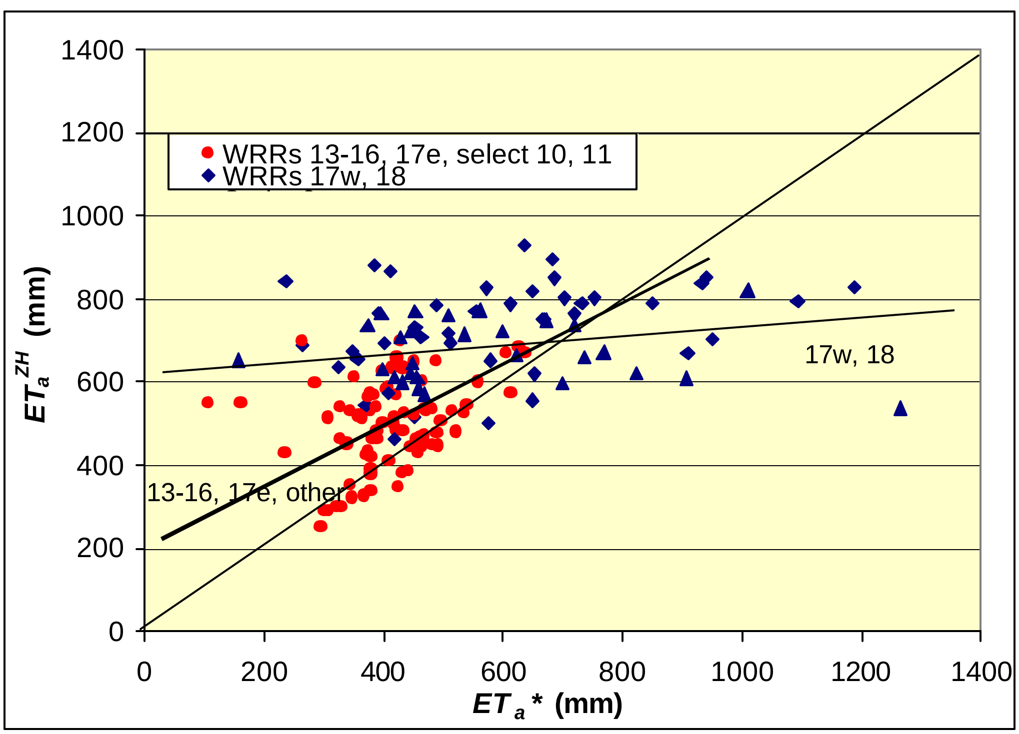

Figure 20. Mean annual ET_a^{ZHadj} versus mean annual ET_a* depth for the 501 test-basins east of the Rockies, post adjustment

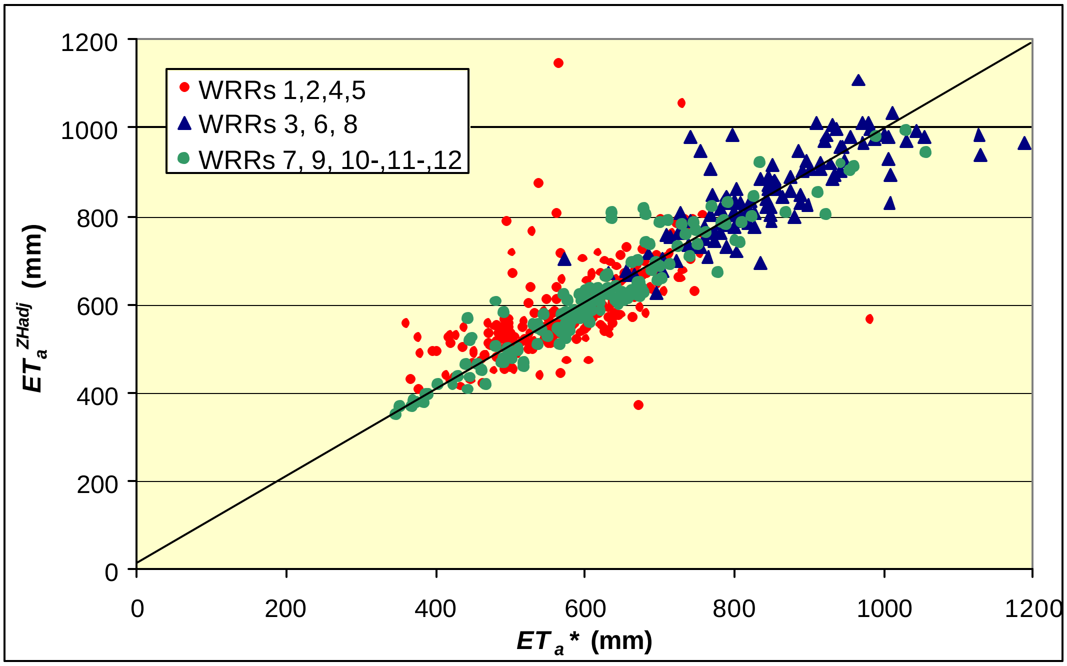

Figure 21. Distributed mean annual ET_a^{ZHadj} generated across the conterminous U.S. over 42 years.

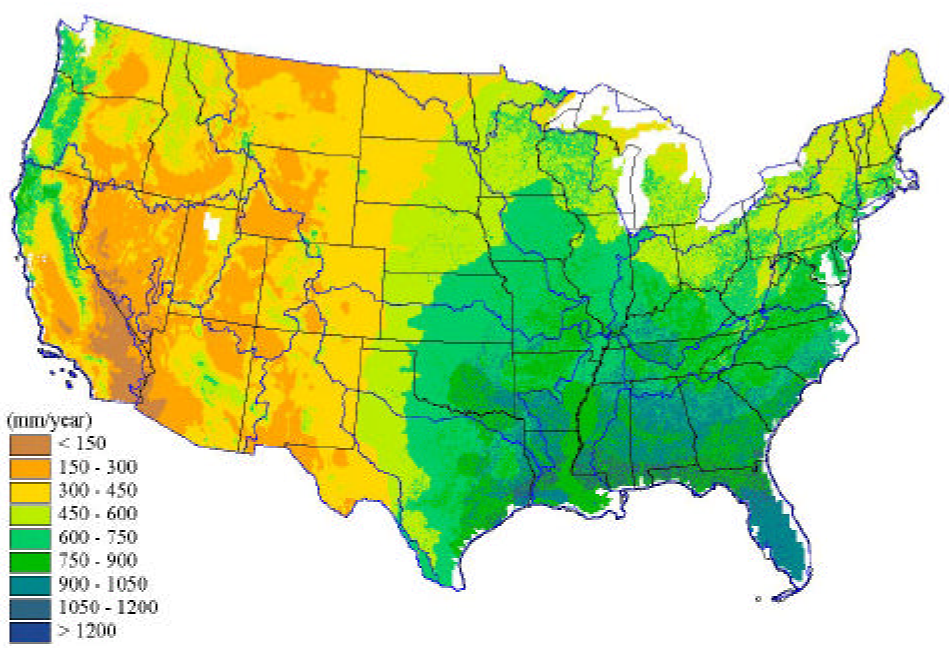

Figure 22. Mean annual ET_a^{ZHadj} versus mean annual ET_a* depth for the 655 test-basins, 1953-94 ($R^2 = 0.73$)

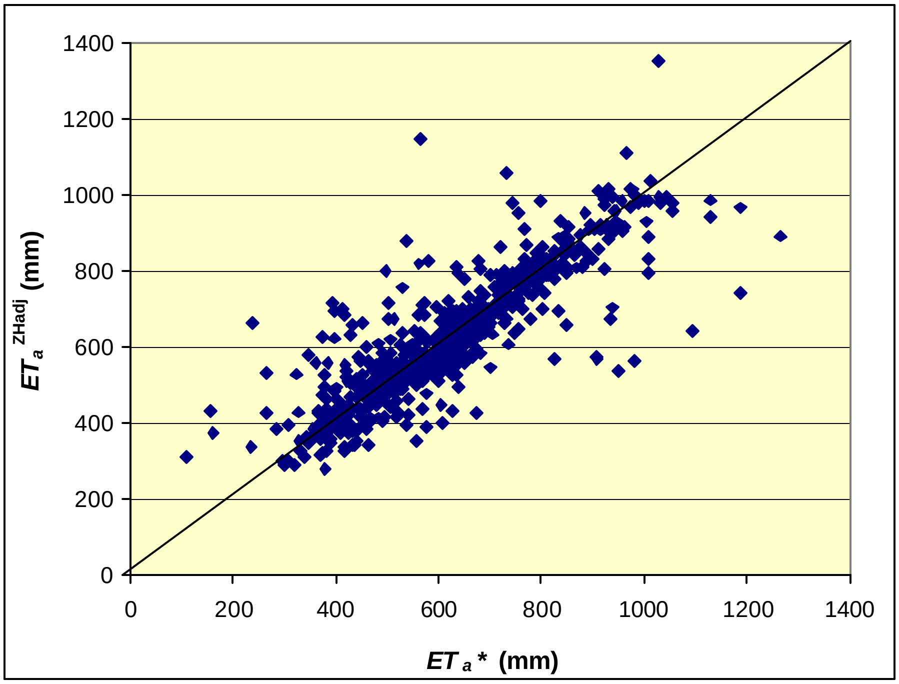

Figure 23. Mean annual ET_a closure errors for Zhang model versus precipitation in 655 test-basins

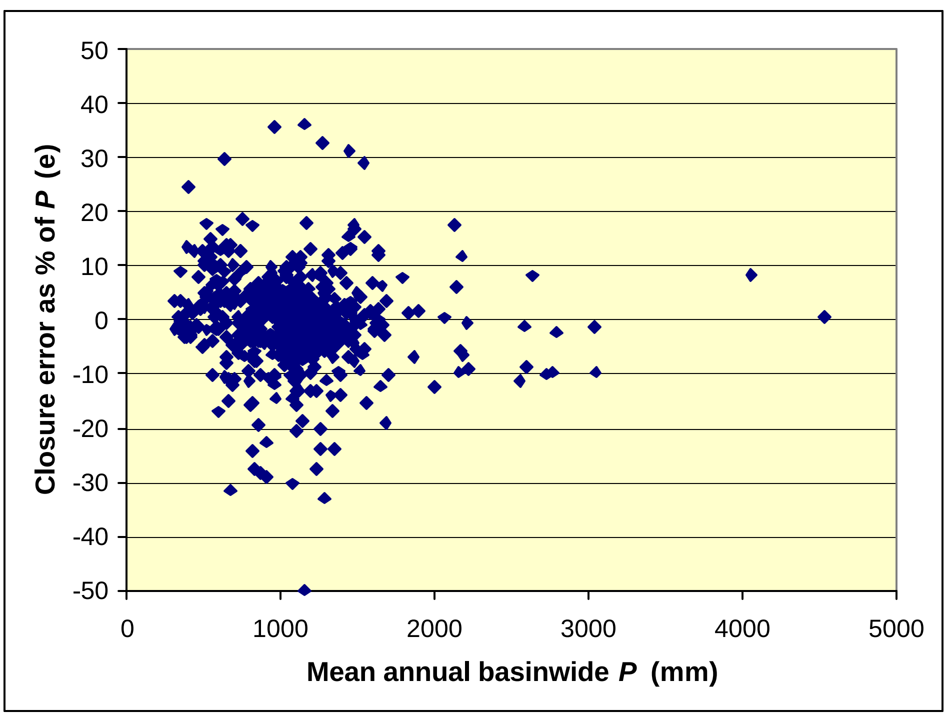

Figure 24. Distributions of mean annual closure errors for the Zhang model (expressed as percentages of mean annual basin-wide precipitation) at the 655 test-basins

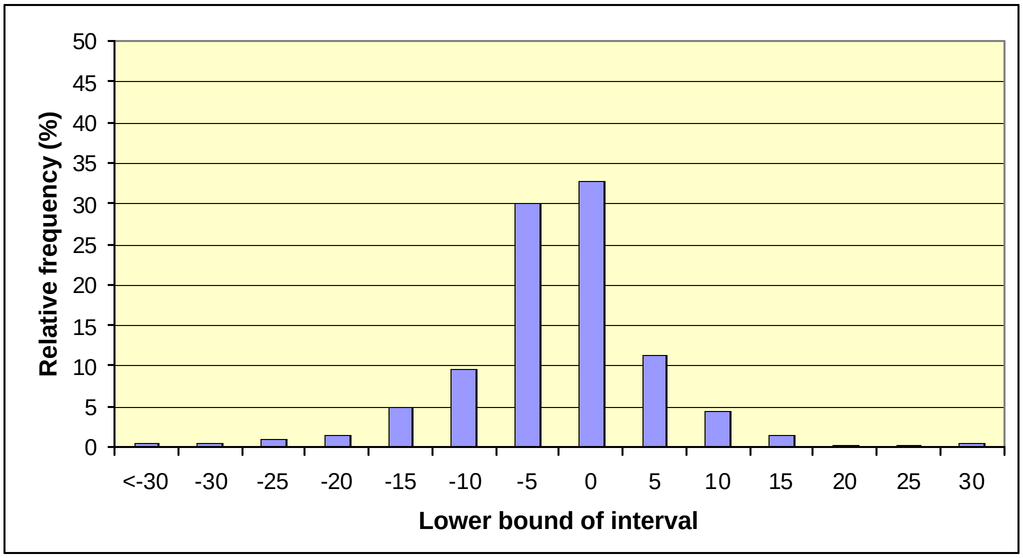

Figure 25. Spatial distribution of mean annual closure errors for the Zhang model (expressed as percentages of mean annual basin-wide precipitation) at the 655 test-basins. Mean annual ET_a closure errors vers us precipitation in 655 test-basins

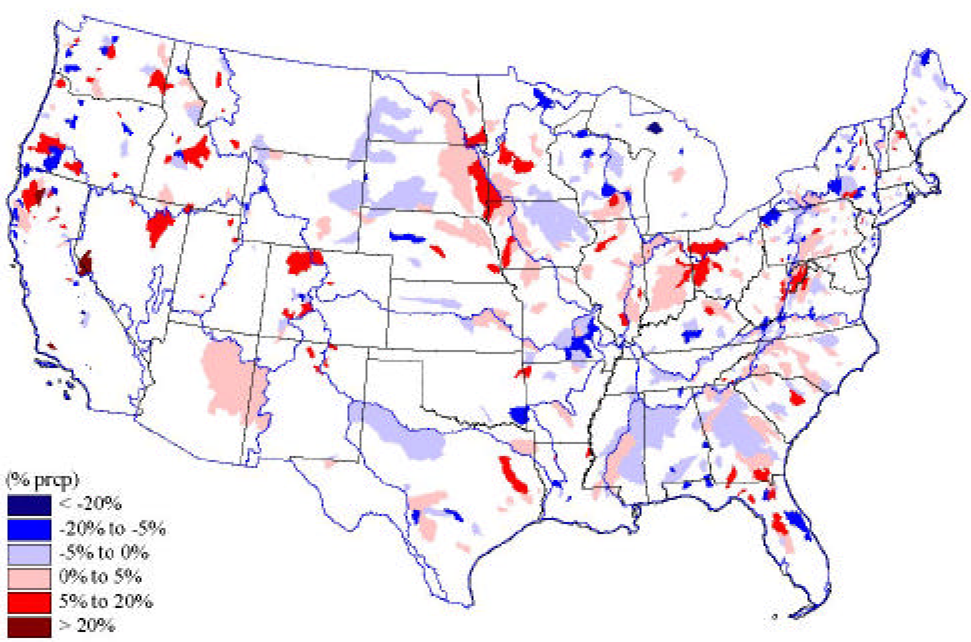

Figure 26. Mean annual water supply for the 18 WRRs of the conterminous U.S. estimated as *R* from USGS gage data for 1951-83, and as Q^{ZH} from the adjusted Zhang model for 1953-83 (R^2 = 0.98)

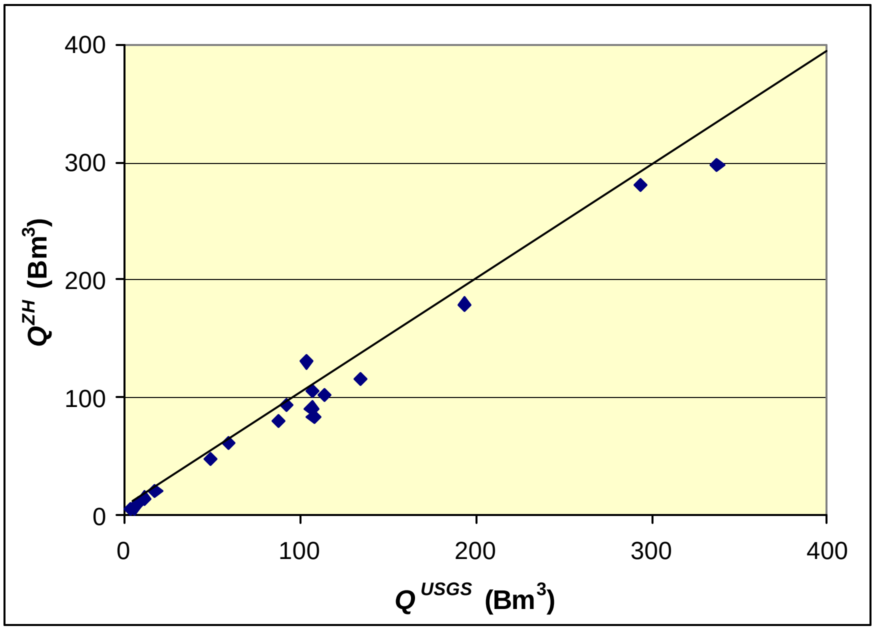

Figure 27. Mean annual water supply for the 18 WRRs of the conterminous U.S. estimated as *R* from USGS gage data for 1951-83, and as $P - ET_a$ with ET_a computed using the calibrated and supplemented AA model and the adjusted Zhang model for 1953-83

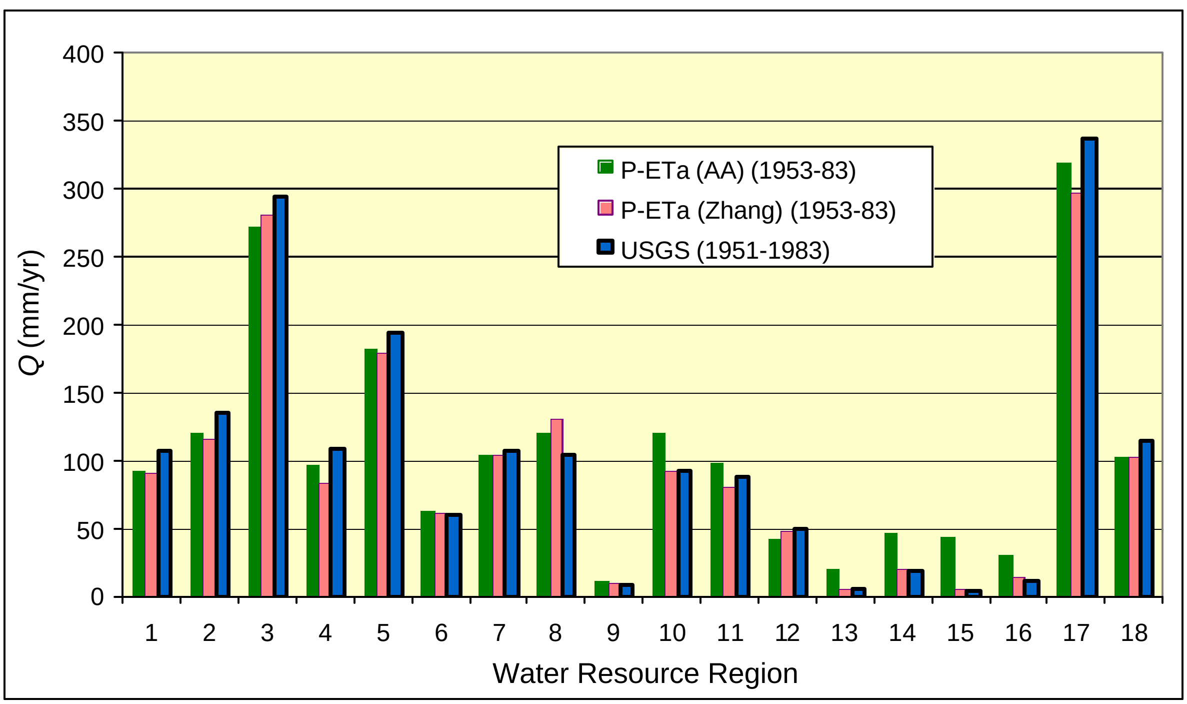

Figure 28. Land ownership classes

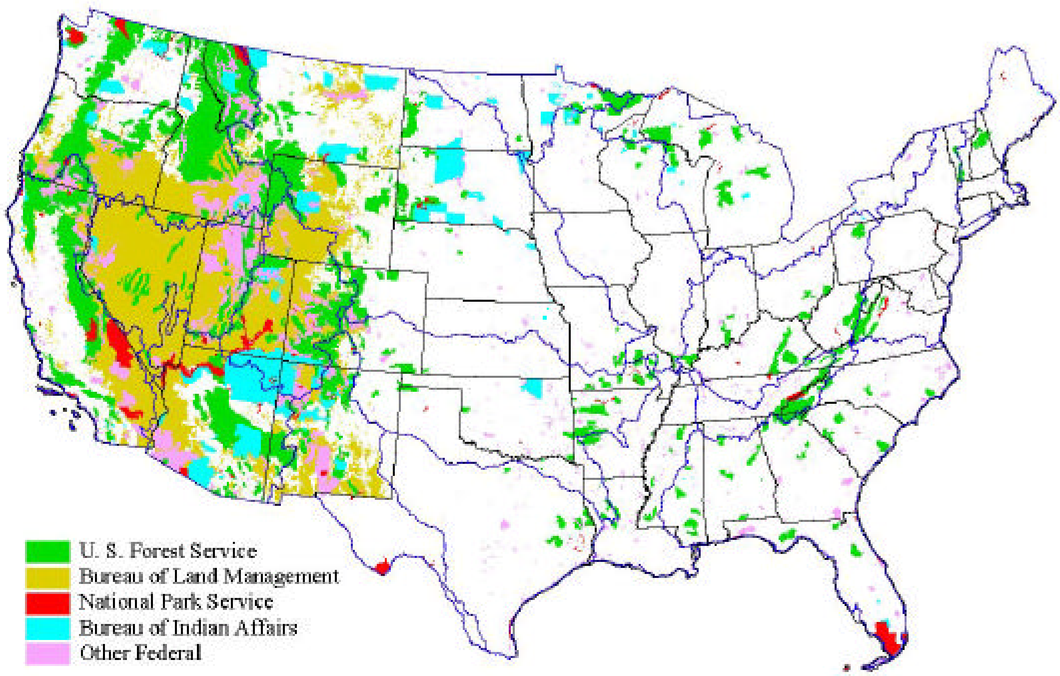

Figure 29. Spatial distribution of five land cover classes

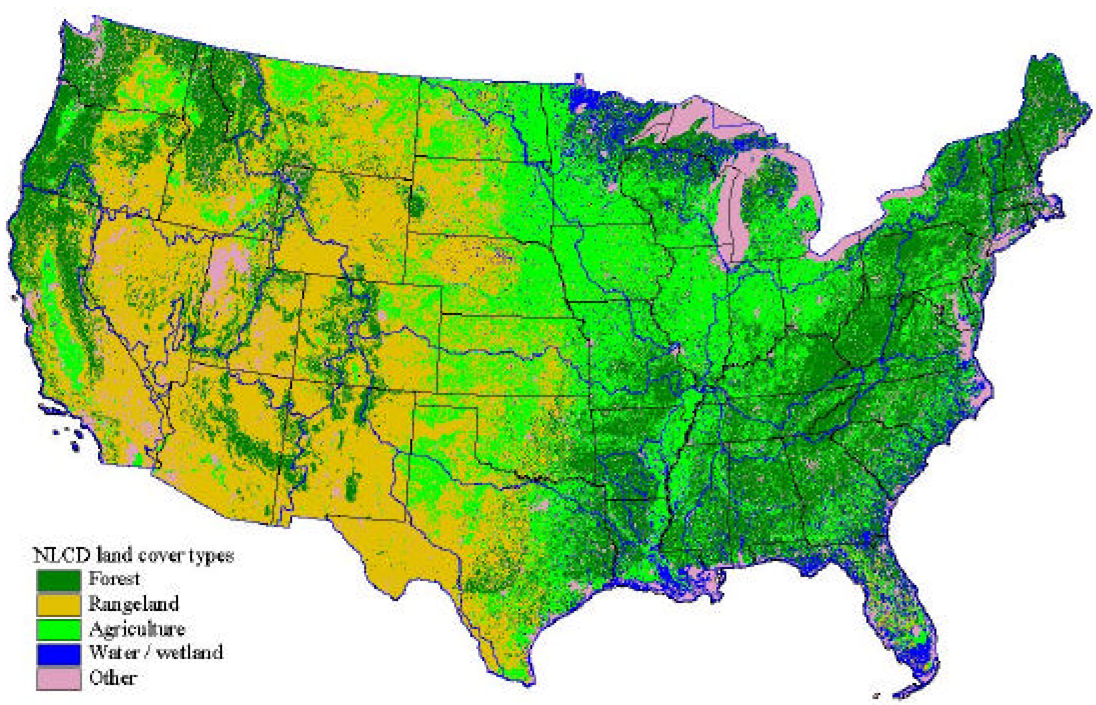

Figure 30. Mean annual ET_a for the conterminous U.S. estimated using the Mixed model

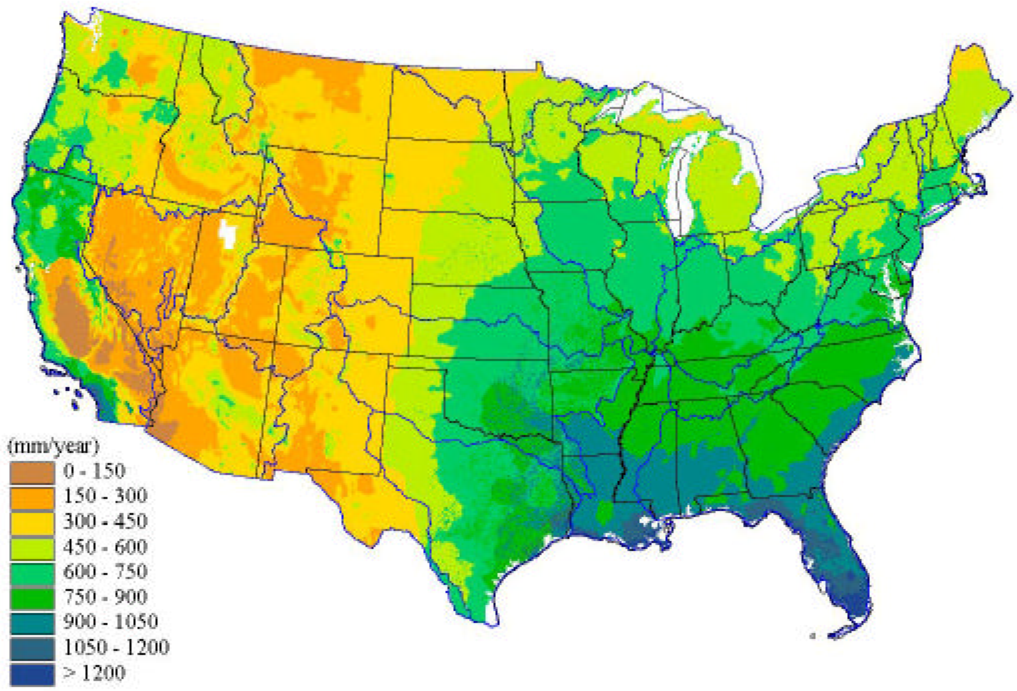

Figure 31. Mean annual contribution to water supply (*Q*) using the Mixed model

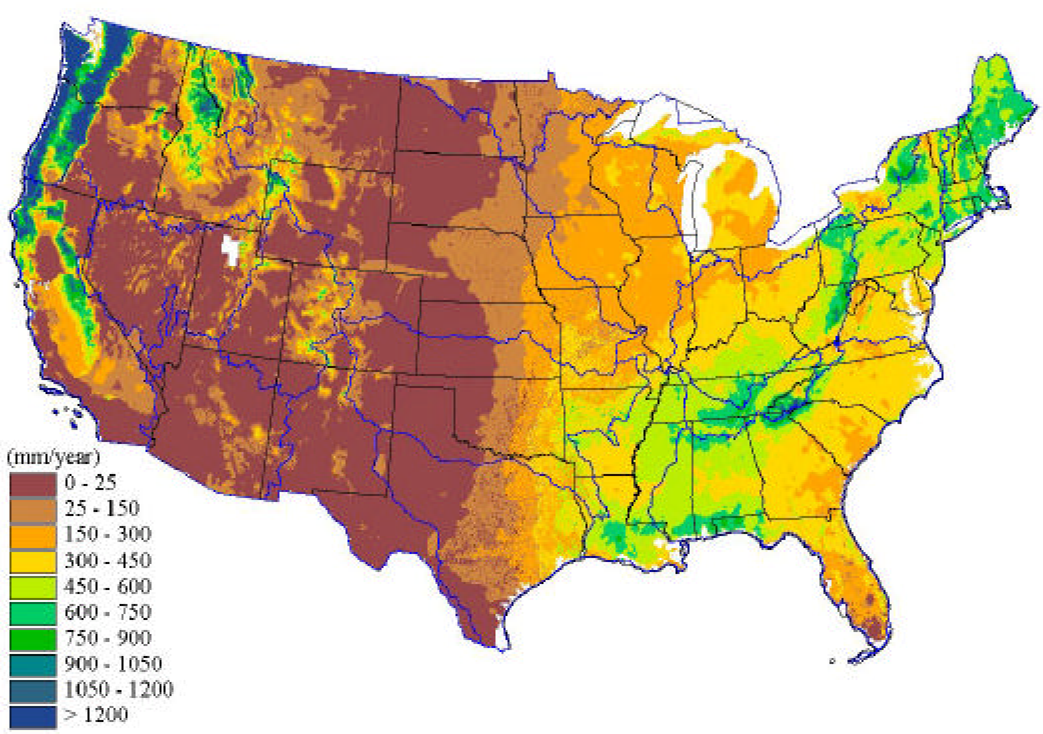

Figure 32. Mean annual water supply originating on NFS land, all other federal land, and state and private land in the conterminous U.S. (see Table 7 for regional definitions)

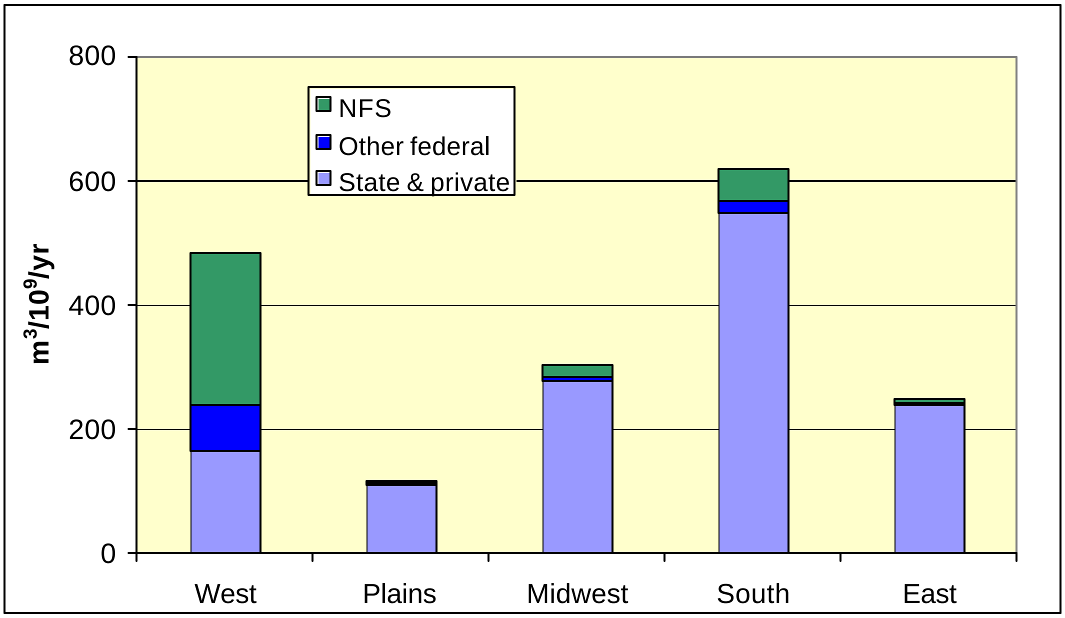

Figure 33. Mean annual water supply originating on federal land and state and private land in the conterminous U.S., by land cover class

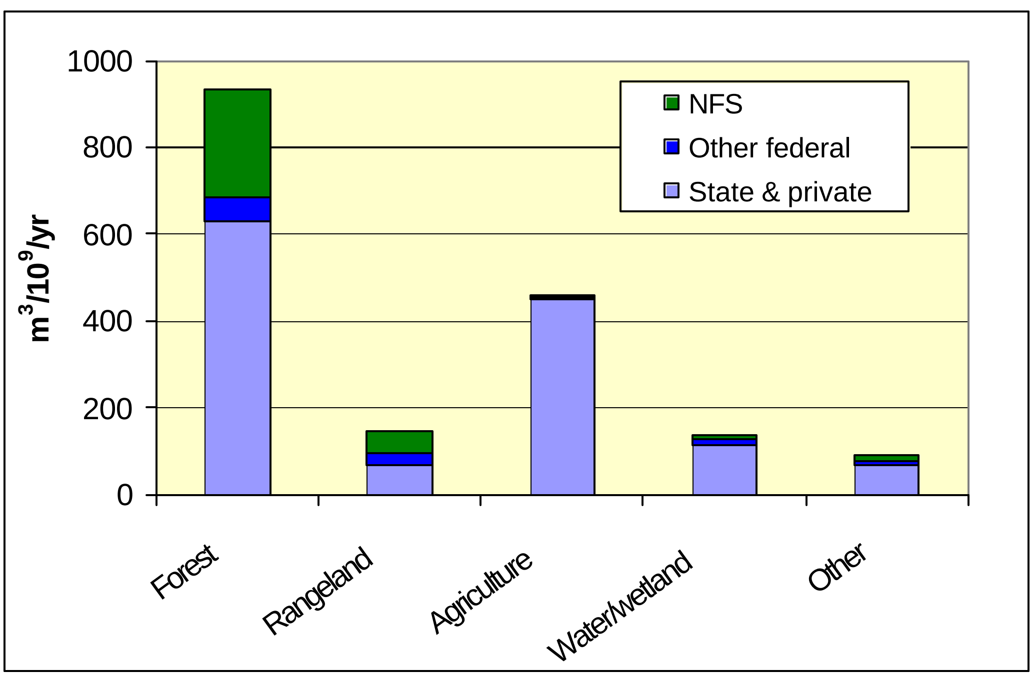

Figure 34. Forest Service regions and national forests and grasslands

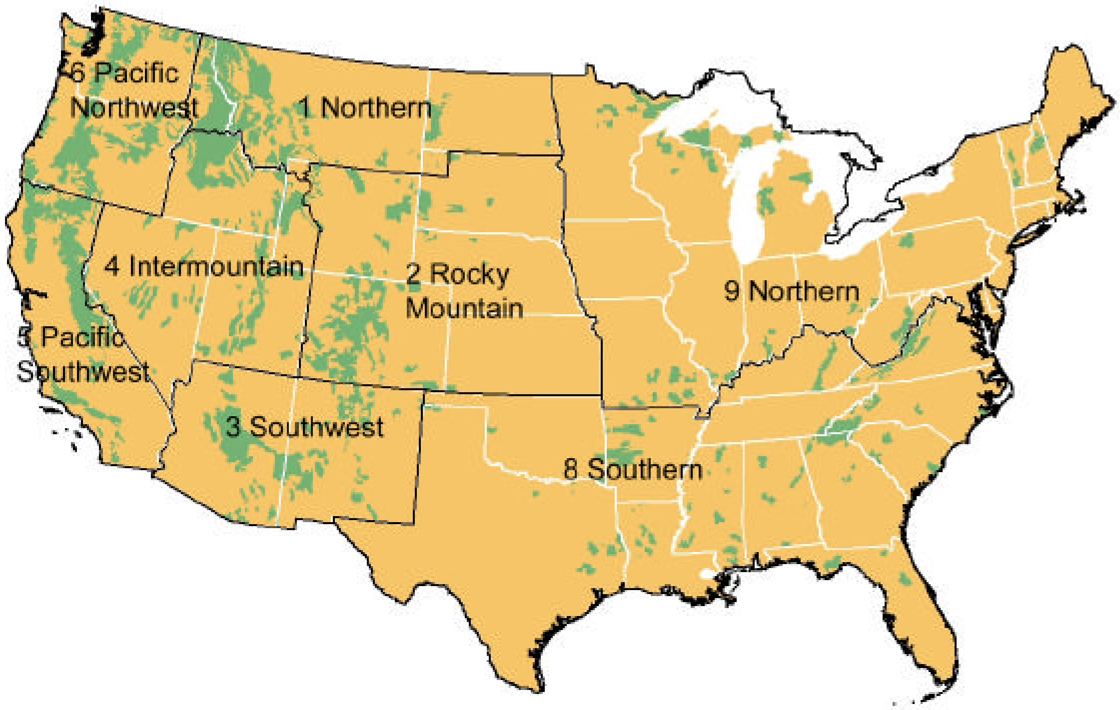

Figure 35. Mean annual water supply originating on NFS land in the conterminous U.S.

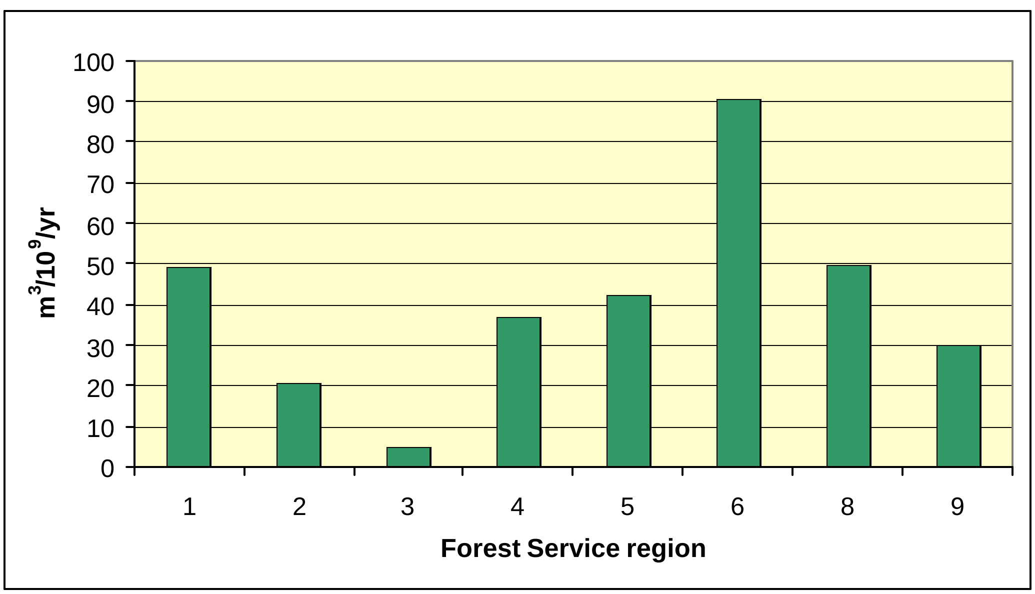

Figure 36. Average annual depth of water supply originating on NFS land in the conterminous U.S.

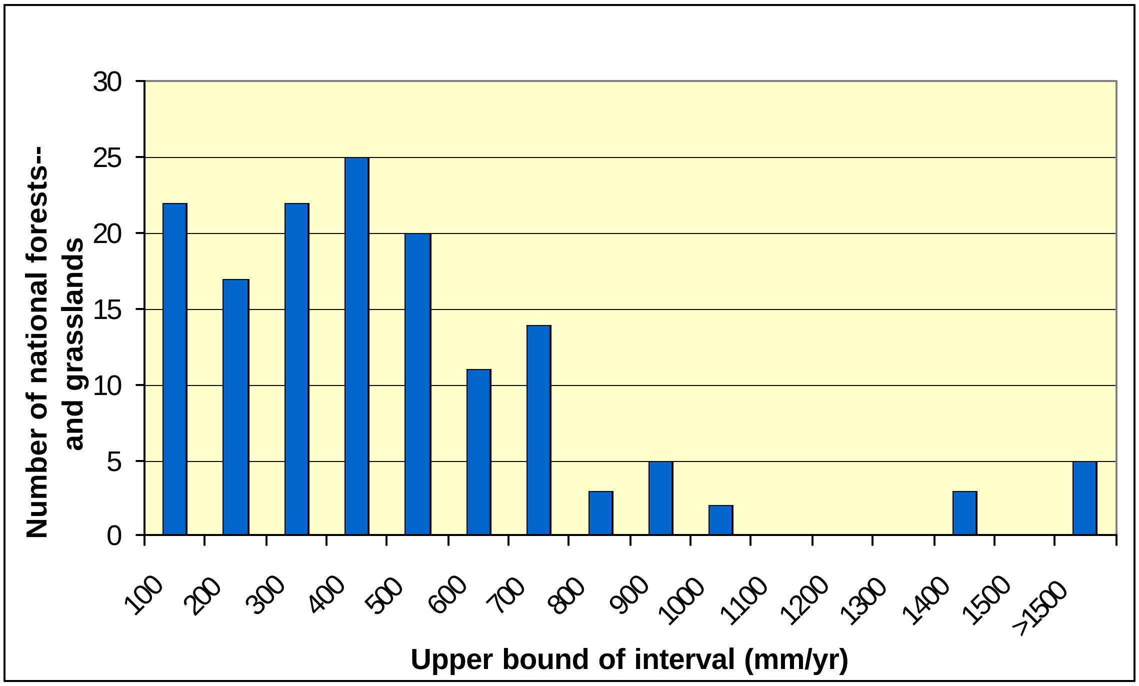

Appendix

Table A-1. Water supply (Mm^3/yr) of the conterminous U.S. by state and land ownership type

State	NFS	BLM	NPS	BIA	Other federal	State & private	Total
AL	2,852	0	45	0	902	66,615	70,414
AR	6,170	0	128	0	1,263	51,323	58,884
AZ	2,517	213	93	949	35	902	4,709
CA	43,317	5,096	5,878	978	1,568	36,210	93,047
CO	15,384	1,509	478	107	75	5,006	22,559
CT	0	0	0	0	10	7,683	7,693
DC	0	0	6	0	3	72	81
DE	0	0	0	0	39	1,950	1,989
FL	2,149	0	303	103	1,982	39,930	44,467
GA	5,329	0	53	0	1,676	52,870	59,928
IA	0	0	1	4	153	31,141	31,299
ID	41,372	3,498	131	1,755	297	14,011	61,064
IL	1,451	0	0	0	272	38,347	40,070
IN	1,005	0	9	0	378	30,345	31,736
KS	0	0	7	92	218	16,147	16,464
KY	4,183	0	204	0	874	44,123	49,384
LA	1,713	0	38	1	1,379	52,485	55,616
MA	2	0	22	0	142	11,922	12,088
MD	0	0	80	0	146	9,393	9,619
ME	199	0	65	79	184	50,343	50,870
MI	6,569	0	76	289	392	39,560	46,886
MN	2,505	0	173	1,145	164	23,839	27,826
MO	3,490	0	130	0	458	46,642	50,720
MS	5,303	0	7	35	828	59,060	65,232
MT	29,805	1,084	4,057	2,855	234	10,584	48,620
NC	8,825	0	1,031	170	1,180	43,123	54,329
ND	84	1	3	78	51	3,871	4,088
NE	47	0	8	155	51	11,239	11,500
NH	2,715	0	0	0	35	11,932	14,682
NJ	0	0	93	0	240	9,343	9,676
NM	2,468	286	11	365	70	2,287	5,486
NV	2,159	2,698	71	46	243	581	5,798
NY	30	0	15	164	420	64,441	65,070
OH	1,432	0	50	0	132	35,130	36,744
OK	714	0	7	864	866	21,318	23,769
OR	43,016	9,212	474	1,049	302	43,727	97,779

PA	1,783	0	84	0	245	59,249	61,362
RI	0	0	0	0	10	1,828	1,838
SC	2,034	0	34	0	621	25,634	28,323
SD	146	2	12	502	26	4,328	5,015
TN	2,949	0	1,036	0	1,864	55,960	61,809
TX	2,373	0	157	3	1,000	52,496	56,029
UT	6,903	801	34	133	27	2,040	9,936
VA	5,398	0	517	0	567	31,673	38,156
VT	1,915	0	0	0	97	11,150	13,162
WA	46,950	42	15,963	2,891	2,227	45,080	113,151
WI	2,177	0	85	668	220	33,257	36,407
WV	4,990	0	132	0	136	25,824	31,081
WY	11,270	1,578	4,542	539	127	3,168	21,224
Total	325,693	26,019	36,342	16,019	24,428	1,339,180	1,767,681

Table A-2. Water supply (Mm^3/yr) of the conterminous U.S. by state and land cover class

State	Forest	Range-land	Agriculture	Water/ wetland	Other	Total
AL	47,321	0	14,545	5,538	3,010	70,414
AR	27,245	69	24,148	6,119	1,303	58,884
AZ	1,927	2,734	5	5	37	4,709
CA	53,574	28,587	6,664	784	3,438	93,047
CO	9,453	11,301	508	224	1,073	22,559
CT	4,466	0	766	771	1,691	7,693
DC	18	0	0	0	63	81
DE	529	0	976	377	106	1,989
FL	15,094	3,947	7,124	12,822	5,481	44,467
GA	35,955	116	13,252	6,133	4,472	59,928
IA	2,393	1,772	25,327	863	945	31,299
ID	38,182	15,756	3,506	863	2,758	61,064
IL	5,691	326	29,864	2,005	2,184	40,070
IN	6,442	135	22,887	999	1,273	31,736
KS	378	5,283	9,834	579	390	16,464
KY	29,720	0	16,728	1,613	1,323	49,384
LA	18,217	278	17,182	17,506	2,434	55,616
MA	7,375	16	643	1,508	2,546	12,088
MD	4,087	0	3,732	971	829	9,619
ME	40,569	291	2,411	5,318	2,281	50,870
MI	19,776	1,004	14,723	9,701	1,681	46,886
MN	6,346	203	12,477	7,995	805	27,826
MO	14,842	209	31,852	2,274	1,542	50,720
MS	32,512	10	21,885	8,506	2,320	65,232

MT	27,805	15,167	2,509	546	2,593	48,620
NC	34,087	0	11,540	6,122	2,580	54,329
ND	9	951	2,899	200	30	4,088
NE	16	3,769	7,178	366	171	11,500
NH	12,072	0	768	1,107	735	14,682
NJ	4,214	0	1,852	1,383	2,226	9,676
NM	2,537	2,826	74	11	38	5,486
NV	998	4,582	34	35	149	5,798
NY	43,133	0	14,240	3,944	3,754	65,070
OH	12,748	8	20,691	1,082	2,214	36,744
OK	6,388	5,887	9,429	1,361	704	23,769
OR	78,293	7,899	6,679	977	3,931	97,779
PA	41,310	0	15,707	1,107	3,237	61,362
RI	1,198	0	53	242	345	1,838
SC	15,671	0	6,336	4,275	2,041	28,323
SD	51	923	3,736	266	40	5,015
TN	38,059	0	18,392	2,663	2,695	61,809
TX	13,023	8,945	24,202	6,101	3,758	56,029
UT	4,261	5,061	178	111	325	9,936
VA	25,743	0	8,817	1,876	1,719	38,156
VT	10,203	13	1,799	773	374	13,162
WA	87,885	7,695	3,032	2,898	11,641	113,151
WI	14,760	155	15,944	4,659	889	36,407
WV	26,548	0	3,639	195	700	31,081
WY	8,077	10,009	391	730	2,017	21,224
Total	931,202	145,925	461,156	136,504	92,893	1,767,681

Table A-3. Water supply (Mm^3/yr) of the conterminous U.S. by state, ownership type, and land cover class group (estimates are tentative and likely to be revised)

State	Federal land		State and private land		Total
	Forest	Non-forest	Forest	Non-forest	
AL	2,909	889	44,412	22,203	70,414
AR	5,992	1,569	21,253	30,070	58,884
AZ	1,886	1,921	41	861	4,709
CA	38,684	18,153	14,890	21,319	93,047
CO	8,206	9,347	1,247	3,759	22,559
CT	2	8	4,464	3,219	7,693
DC	3	6	15	57	81
DE	0	39	529	1,421	1,989
FL	2,013	2,524	13,081	26,849	44,467
GA	5,891	1,168	30,064	22,805	59,928

IA	28	130	2,365	28,776	31,299
ID	31,937	15,116	6,245	7,767	61,064
IL	873	850	4,818	33,529	40,070
IN	971	421	5,471	24,874	31,736
KS	8	309	370	15,777	16,464
KY	4,673	588	25,047	19,076	49,384
LA	1,781	1,350	16,435	36,050	55,616
MA	77	89	7,298	4,624	12,088
MD	118	108	3,969	5,423	9,619
ME	440	88	40,129	10,214	50,870
MI	4,815	2,510	14,961	24,599	46,886
MN	1,570	2,417	4,776	19,063	27,826
MO	2,937	1,141	11,905	34,737	50,720
MS	3,727	2,445	28,785	30,275	65,232
MT	25,873	12,163	1,932	8,652	48,620
NC	9,614	1,593	24,473	18,649	54,329
ND	0	216	9	3,863	4,088
NE	0	261	16	11,223	11,500
NH	2,645	105	9,427	2,505	14,682
NJ	171	162	4,044	5,299	9,676
NM	1,959	1,240	578	1,709	5,486
NV	964	4,253	35	547	5,798
NY	439	190	42,694	21,747	65,070
OH	1,290	324	11,459	23,671	36,744
OK	818	1,633	5,570	15,747	23,769
OR	46,387	7,666	31,905	11,821	97,779
PA	1,978	135	39,333	19,916	61,362
RI	1	9	1,197	632	1,838
SC	2,005	684	13,666	11,968	28,323
SD	43	645	8	4,320	5,015
TN	4,792	1,057	33,267	22,693	61,809
TX	1,606	1,928	11,418	41,078	56,029
UT	3,650	4,247	611	1,428	9,936
VA	5,616	867	20,128	11,546	38,156
VT	1,870	141	8,333	2,817	13,162
WA	53,281	14,791	34,604	10,476	113,151
WI	2,104	1,046	12,655	20,601	36,407
WV	4,848	410	21,700	4,124	31,081
WY	7,876	10,180	202	2,966	21,224
Total	299,369	129,132	631,833	707,347	1,767,681